

A T cell redirection platform for co-targeting dual antigens on solid tumors

Leonie Enderle, Karim H. Shalaby, Maryna Gorelik, Alexander Weiss, Levi L. Blazer, Marcin Paduch, Lia Cardarelli, Anthony Kossiakoff, Jarrett J. Adams & Sachdev S. Sidhu

To cite this article: Leonie Enderle, Karim H. Shalaby, Maryna Gorelik, Alexander Weiss, Levi L. Blazer, Marcin Paduch, Lia Cardarelli, Anthony Kossiakoff, Jarrett J. Adams & Sachdev S. Sidhu (2021) A T cell redirection platform for co-targeting dual antigens on solid tumors, mAbs, 13:1, 1933690, DOI: [10.1080/19420862.2021.1933690](https://doi.org/10.1080/19420862.2021.1933690)

To link to this article: <https://doi.org/10.1080/19420862.2021.1933690>



© 2021 The Author(s). Published with license by Taylor & Francis Group, LLC.



[View supplementary material](#)



Published online: 30 Jun 2021.



[Submit your article to this journal](#)



Article views: 2163

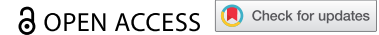


[View related articles](#)



[View Crossmark data](#)

REPORT



A T cell redirection platform for co-targeting dual antigens on solid tumors

Leonie Enderle^{a,b,*}, Karim H. Shalaby^{a,b,*}, Maryna Gorelik^{a,b}, Alexander Weiss^{a,b}, Levi L. Blazer^{a,b}, Marcin Paduch^c, Lia Cardarelli^{a,b}, Anthony Kossiakoff^{c,d}, Jarrett J. Adams^{a,b}, and Sachdev S. Sidhu^{a,b}

^aDonnelly Centre, University of Toronto, Toronto, Canada; ^bDepartment of Molecular Genetics, University of Toronto, Toronto, Canada; ^cInstitute for Biophysical Dynamics, Gordon Center for Integrative Science, Chicago, USA; ^dDepartment of Biochemistry and Molecular Biology, University of Chicago, Chicago, USA

ABSTRACT

In order to direct T cells to specific features of solid cancer cells, we engineered a bispecific antibody format, named **D**ual **A**ntigen **T** cell Engager (DATE), by fusing a single-chain variable fragment targeting CD3 to a tumor-targeting antigen-binding fragment. In this format, multiple novel paratopes against different tumor antigens were able to recruit T-cell cytotoxicity to tumor cells *in vitro* and in an *in vivo* pancreatic ductal adenocarcinoma xenograft model. Since unique surface antigens in solid tumors are limited, in order to enhance selectivity, we further engineered “double-DATES” targeting two tumor antigens simultaneously. The double-DATE contains an additional autonomous variable heavy-chain domain, which binds a second tumor antigen without itself eliciting a cytotoxic response. This novel modality provides a strategy to enhance the selectivity of immune redirection through binary targeting of native tumor antigens. The modularity and use of a common, stable human framework for all components enables a pipeline approach to rapidly develop a broad repertoire of tailored DATES and double-DATES with favorable biophysical properties and high potencies and selectivities.

ARTICLE HISTORY

Received 27 September 2020
Revised 18 May 2021
Accepted 19 May 2021

KEYWORDS

Antibody/immunotherapy/
pancreatic cancer/solid
tumors/T-cell redirection/
CD133/EPHA2/EPCAM/
EPHB2/dual targeting



Introduction

Antibody-based immunotherapies have shown great promise in cancer treatment.^{1,2} These therapies are centered on the stimulation of antitumor immunity and targeting of tumor surface antigens with antibody-based modalities. In particular, the enhancement of anti-cancer T-cell responses through checkpoint inhibition, or redirection to tumors through bispecific T-cell engagers (BiTEs) or chimeric antigen receptors (CARs), has shown promise especially in treating blood cancers.³ Despite this progress, solid tumors remain challenging targets for cancer immunotherapeutics⁴ due to factors such as limited access of biologics and immune cells to tumors,^{5,6} the immunosuppressive tumor microenvironment,⁷ loss of tumor antigen from the cell surface, and development of resistance through alternative signaling pathways.^{8,9} For example, checkpoint inhibition may have limited efficacy in “cold” tumors, in which there are few tumor-infiltrating lymphocytes, or in “non-immunogenic” tumors that are not recognized by T cells due to the absence of cancer cell-specific ‘neo-antigens’.^{10–12}

In such cases, bispecific antibodies can mitigate these problems by recruiting T cells and directing their cytotoxic activity to tumors. Antibodies that are engineered for such T-cell redirection rely on an effective combination of paratopes in order to evoke T-cell activation specifically upon binding to a tumor cell.^{13–16} T-cell binding and activation are typically achieved using a single-chain variable fragment (scFv) that engages the T-cell co-receptor CD3. Two T-cell-redirecting molecules have been approved as

human cancer therapies, and many more are in development.^{3,17–19} T-cell redirection has been used effectively to treat blood cancers, but there are currently no approved CD3-engaging bispecific antibodies for solid tumors, for which targeting, access, and sustained activity remain major challenges, as discussed in reviews by Slaney et al.⁴ and Labrijn et al.¹³ Several co-therapies are being explored in combination with T-cell engagers to enhance T-cell infiltration in solid tumors and to overcome the immunosuppressive tumor microenvironment, such as oncolytic viruses and checkpoint blockade.¹³ Compact BiTE molecules, built with tandem scFvs, are favorable for the establishment of effective immune synapses and efficient T-cell activation^{20,21} and may improve access to solid tumors.²² However, scFvs are prone to intra- and intermolecular mispairing of domains and consequent aggregation, and thus, tandem-scFv BiTEs often suffer from low production yields, molecular heterogeneity, and low stability in serum.^{23–25} Moreover, both approved molecules, the BiTE blinatumomab (Blinxtyo; DrugBank entry DB09052)¹⁷ and the bispecific IgG catumaxomab (REMOVAB; DrugBank entry DB06607),¹⁸ and many of the antibodies in development, contain nonhuman frameworks that pose an inherent risk of eliciting immunogenicity in humans. Therefore, multiple limiting factors, including developability, serum stability, and immunogenicity, have hampered successful translation of T-cell-redirecting antibodies to the clinic.

Another fundamental challenge to T-cell redirection is the limited availability of truly tumor-specific antigens.²⁶ BiTEs, for instance, target individual tumor antigens, but with the

CONTACT Sachdev S. Sidhu  sachdev.sidhu@utoronto.ca  Donnelly Centre, University of Toronto, Toronto, Canada; Department of Molecular Genetics, University of Toronto, Toronto, Canada

*Co-authors.

 Supplemental data for this article can be accessed on the [publisher's website](#).

© 2021 The Author(s). Published with license by Taylor & Francis Group, LLC.

This is an Open Access article distributed under the terms of the Creative Commons Attribution-NonCommercial License (<http://creativecommons.org/licenses/by-nc/4.0/>), which permits unrestricted non-commercial use, distribution, and reproduction in any medium, provided the original work is properly cited.

exception of rare mutations in tumor surface proteins, such as the deletion variant EGFRvIII in glioblastoma,²⁷ there are few antigens that are uniquely displayed on tumors to enable targeting without affecting healthy tissues in patients (on-target, off-tumor effects). This is especially true for solid tumors such as pancreatic cancers, where oncogenic transformation is driven by mutations in intracellular oncogenes such as KRAS.²⁸ KRAS oncogenic transformation induces changes in the composition of the native cell-surface proteins, or “surfaceome,” which facilitates the growth and metastasis of tumors.²⁹ Similarly, tumor-initiating cell (TIC) populations have proven to be challenging targets, as TICs commonly share surface antigens with adult stem cell populations, prohibiting the safe application of cytotoxic immunotherapies.

Recruiting T cells to malignant cells by targeting a single tumor antigen may be sufficient to treat some cancers, but targeting specific combinations of tumor-associated antigens (TAAs) to improve selectivity for tumor over normal tissues could have much broader applications in cancer therapy. There is evidence that co-targeting TAAs can augment the selectivity and efficacy of T-cell-redirecting antibodies and CAR-T therapies.^{25–32} Innovative approaches that use “AND” logic, i.e. that require simultaneous binding of antibodies to more than one tumor antigen for T-cell activation, are successfully being developed.^{33,34} On-target, off-tumor T-cell activity can also be mitigated by creating increased binding strength through avidity,³⁵ as demonstrated, for instance, by adding two low-affinity paratopes targeting HER2 protein for selective killing of tumor cells with high HER2 receptor density.³⁶ Herein, a secondary goal of ours was to develop a single molecular entity that would co-target distinct TAAs and increase binding strength to cells co-expressing these targets, in order to enable more selective T-cell redirection to solid tumors such as pancreatic cancer.

To address some of the challenges facing the application of T-cell-redirecting antibodies for solid tumors, we used a modular synthetic antibody format, termed a Dual Antigen T-cell Engager (DATE), which possesses robust biophysical properties and can be efficiently customized for specific indications (Figure 1). For T-cell recruitment, we used the highly validated framework from the anti-HER2 therapeutic antibody trastuzumab to humanize the murine anti-CD3 antibody murononab and converted it into scFv format. For targeting of tumor cells, we used an antigen-binding fragment (Fab) library, built on the same trastuzumab framework, to rapidly

isolate Fabs that recognized diverse tumor antigens (EPHA2, EPHB2, CD133 and EPCAM) by phage display. Due to the modular nature of the antibody structure, Fabs could be efficiently coupled to the anti-CD3 scFv to assemble DATEs for selective tumor cell killing. A similar Fab-scFv fusion protein has been previously described to enable co-binding of two targets.³⁷ By fusing an additional autonomous variable heavy-chain (VH) domain to the Fab, we constructed “double-DATEs” (d-DATEs) with enhanced specificity achieved by targeting two distinct TAAs. The use of a single stable framework, and different antibody fragment formats (scFv, Fab and VH), ensured that DATEs and d-DATEs could be rapidly assembled and purified in high yields as molecules with predictable binding and effector functions. Going forward, the modular nature of DATEs and their compatibility with synthetic antibody discovery platforms will facilitate a pipeline approach to efficiently produce customized bi- and tri-specific T-cell-engaging human antibodies for targeting cancer cells with high affinity and potency.

Materials and methods

Antibody selections:

The phage-displayed synthetic library F/H and library J-D were used to select Fabs or VH domains, respectively, that bound to EPH receptors, as described.³⁸ Briefly, His-tagged EPHA2 or EPHB2 purified from SF9 insect cells³⁹ or Fc-tagged ectodomain (ECD) proteins (R&D Systems) were immobilized on Maxisorp Immuno plates (ThermoFisher, #12-565-135) and used for positive binding selections with library phage pools that were first exposed to similarly immobilized Fc protein to deplete nonspecific binders. After four rounds of binding selections, clonal phage was prepared and evaluated by phage ELISA.⁴⁰ Clones that displayed at least 10-fold greater signal for binding to antigen compared with Fc were considered to be specific binders that were subjected to further characterization. The CD133-targeting paratope has been described previously (US patent application #20,190,330,362)

Engineering of DATEs and d-DATEs:

DATE and d-DATE expression constructs were generated by cloning light and heavy chains into mammalian expression vectors with a CMV promoter. DATEs consist of a Fab heavy

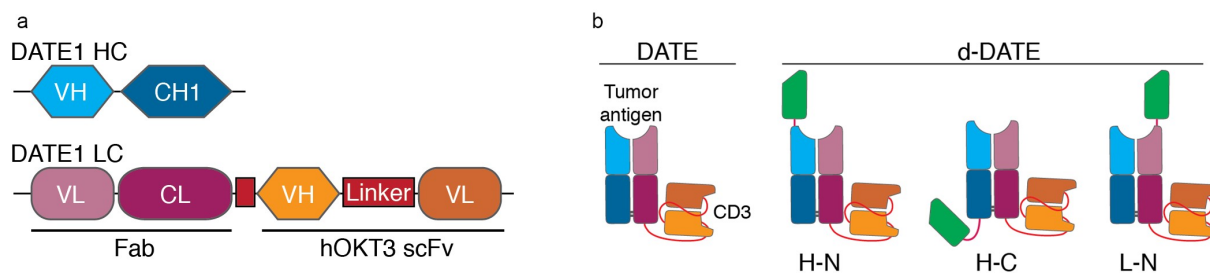


Figure 1. DATE and d-DATE designs. **(A)** Schematic of the two chains that assemble to form a DATE. The first chain is a Fab heavy chain (HC), which consists of a VH domain (light blue) and a CH1 domain (dark blue). The second chain contains a Fab light chain (LC), which consists of a VL domain (light purple) and a CL domain (dark purple), fused to a hOKT3 scFv, which consists of a VH domain (light orange) and a VL domain (dark orange) connected by a linker (red). **(B)** Molecular architecture of DATE and d-DATE proteins. The Fab and hOKT3 scFv are colored as in (A) and the additional VH domain in d-DATEs is colored green.

chain (VH-CH1) and a light chain containing a Fab light chain (VL-CL) followed by a linker (amino-acid sequence GGGGS) and the hOKT3 scFv. The hOKT3 scFv was attached in the VH-VL orientation, where VH and VL are linked with a flexible long linker (GTTAASGSSGGSSGA), which facilitates scFv formation. D-DATs were generated by fusing a VH domain either N-terminally to the DATE heavy chain (H-N) or light chain (L-N), or C-terminally to the DATE heavy chain (H-C), either using one (subscript S) or two (subscript L) GGSGG linker repeats. The H-N format with a single GGSGG linker was used for all experiments unless otherwise specified. Expression constructs contain antibody ORF modules as follows:

DATE HC: VH-CH1

DATE LC (hOKT3 in bold): VL-CL-GGGGS-**VH-GTTAASGSSGGSSGA-VL**

d-DATE H-N_S (VH domain in bold): **VH-GGSGG-VH-CH1**

d-DATE H-C_S (VH domain in bold): **VH-CH1-GGSGG-VH**

Western blot and Coomassie analysis:

Western blot analysis was performed using lysates collected from cells treated with RIPA buffer for 10 min on ice. Cellular debris was pelleted by centrifugation and supernatants were heated to 95°C with sample buffer + 5% β-mercaptoethanol for 3 min. Samples were separated by SDS PAGE (BioRad MiniProtein TGX gradient gels), transferred to PVDF membranes, and blocked in 5% skim milk. The following antibodies were used for detection: EPHA2 D4A2 (CellSignaling #6997 T), EPHB2 1A6C9 (ThermoFisher #37-1700), GAPDH-HRP H12 (Santa Cruz #sc-166,574 HRP), GAPDH (CellSignaling #2118), anti-rabbit-HRP (CellSignaling #7074), anti-mouse-HRP (CellSignaling #7076), anti-hCD133 clone7 (Biolegend #372,802), anti-CD133 clone 133-1 (in house), Goat Anti-Human Kappa-HRP (Southern Biotech #2060-05). For Coomassie gels, 3 μg or 5 μg protein were heated to 95°C with sample buffer (nonreducing conditions) or sample buffer + 5% β-mercaptoethanol for 3 min, separated by SDS PAGE (BioRad MiniProtein TGX gradient gels), stained (Coomassie Blue in 10% acetic acid + 50% methanol in water), destained (10% acetic acid, 50% methanol in water) and imaged.

Antibody production:

IgGs, DATs, and d-DATs were produced using the human Expi293 expression system (ThermoFisher # A14635). Expi293F cells were maintained in Expi293 expression medium (LifeTech A1435102) on orbital shaking platforms (25 mm, 125 rpm) at 37°C and 8% CO₂.

For protein production, Expi293 cells were grown to a density of approximately 2.5×10^6 cells/mL and heavy- and light-chain DNA was transfected at 1:1 ratios using FectoPro transfection reagent (Polyplus Transfection #116-010). After 5 d the cell supernatant was harvested by centrifugation, incubated with rProteinA Sepharose FastFlow overnight (GE Healthcare #GE17-1279-03), and collected in Polyprep columns for purification. ProteinA beads with bound antibodies

were washed with PBS, antibodies eluted in Pierce Elution Buffer (ThermoFisher #21,004), neutralized with TRIS pH8.0 and buffer exchanged into DPBS using Amicon centrifugal concentrators (30 K cutoff, Millipore). Endotoxin levels of the final preparation were measured (Charles River, Endosafe) and protein concentrations were determined by absorbance measurements at 280 nm (Biotek Epoch).

ELISA:

ELISAs were performed in 384-well Maxisorp plates coated overnight with 1 μg/mL recombinant antigen. Plates were blocked with 0.5% bovine serum albumin (BSA) for 1 hour at room temperature and washed with PBS + 0.05% Tween20. The antibody was added at 100 nM unless specified otherwise and allowed to bind for 60 min at room temperature. Plates were washed with PBS + 0.05% Tween20 and binding was detected with anti-kappa HRP antibody (1:5000, Southern Biotech #2060-05). The following antigens were used: hEPA2 (R&D 3035-A2), mEPA2 (Sino 50,586-M08H), hEPHB2 (R&D 5189-B2), mEPHB2 (R&D 467-B2-200), Gaussia luciferase (Nanolight #321-100), hEPCAM (R&D 9277-EP). Human IFN-γ was quantified in cell culture supernatants using the Human IFN-γ DuoSet ELISA (R&D DY285B-05), following the manufacturer's instructions. Standard curves were fitted with a 4PL fit and sample measurements were interpolated accordingly.

Biolayer interferometry:

All kinetic data were generated from experiments that were performed using BLI on an Octet HTX instrument (Forte Bio). All experiments were performed using a buffer consisting of PBS supplemented with 0.05% Tween-20 and 1% BSA and a shaking speed of 1000 rpm. Kinetic measurements were performed by immobilizing Eph antigens (described above) to approximately 0.3 nm on AR2G sensors, followed by quenching remaining reactive sites with ethanolamine. Sensors were exposed to serial dilutions of the antibody for 300 seconds, followed by a disassociation time of 300 seconds. Kinetic values were determined using the Octet Data Analysis Software using a global fitting algorithm. Epitope binning experiments were performed using BLI in a similar manner. Recombinant human EphA2 ECD was immobilized via amine coupling to AR2G sensors to provide a signal change of approximately 0.3 nm. The competitive binding assay was performed by saturating the sensors with a primary antibody (100 nM) and then transferring them to wells containing a competing antibody (100 nM). The response provided by the competing antibody after 15 seconds of contact time with the sensors was quantified. Recombinant Human EphB2-Fc was captured on antihuman IgG Fc (AHQ) sensors to provide a signal change of approximately 0.7 nm. The competitive binding assay was performed by saturating the sensors with a primary antibody (200 nM) for 600 s and then transferring them to wells containing a competing antibody or ligand (200 nM) for 600 s. Endpoint response to competing analytes was measured and normalized based upon the antigen-

unblocked response (i.e. an assay in which the sensor was exposed to a nonbinding control IgG during the primary saturation step).

Size exclusion chromatography:

Analytical SEC of DATES or d-DATES was performed by applying 50 µg protein at 1 mg/mL on a TSKgel BioAssist G3SWxl column (Tosoh Bioscience) connected to an NGC chromatography system (BioRad) in a mobile phase of PBS and monitoring elution at 215 and 280 nm. Preparative SEC was performed by separating 1 mg of Protein A purified d-DATES over a Superdex200 column (GE Healthcare) in PBS. Fractions corresponding to monodispersed DATE or d-DATES were pooled and concentrated using Amicon spin concentrators (30 K cutoff, Millipore). Monodispersity was confirmed via the analytical SEC as described above.

Cell culture:

Cell line HCT116 was obtained from the American Tissue Type Collection (ATCC). Cell line KP4 was obtained from the Japan Health Sciences Foundation (JHSF). RCC243 is a patient-derived renal clear cell carcinoma line previously described.⁴¹ HEK293T cells stably expressing CD133-Green Fluorescent Protein (GFP) have been described previously.⁴² Patient tumor-derived pancreatic ductal adenocarcinoma cell lines GP5A, GP13A, GP14A, and GP16A were a generous gift from Dr. David Hedley, Toronto, Canada, and described previously.⁴³ Cell lines were maintained as follows: KP4 cell lines in RPMI (ThermoFisher Cat# A1049101) supplemented with 10% FBS, HCT116 cells in McCoy's 5A (ThermoFisher Cat# 16600-108) supplemented with 10% FBS, RCC243 cells in IMDM (ThermoFisher Cat# 12440061) supplemented with 10% FBS, HEK293T cells in DMEM (ThermoFisher Cat# 11995073), GP5A, GP13A, GP14A in DMEM/F12 1:1 (ThermoFisher Cat# 11320033) supplemented with 10% FBS, GP16A in DMEM/F12 1:1 (ThermoFisher Cat# 11320033) supplemented with 2.5% FBS, GP9A in RPMI (Cat# 11875119) supplemented with 10% FBS. All adherent lines were maintained at 37°C and 5% CO₂.

Cell line development:

KP4, HCT116, and RCC243 cells stably expressing firefly luciferase-GFP were generated by lentiviral transduction. Lentivirus was generated by transfection of HEK293T cells with packaging plasmid psPAX2 (Addgene #12260), envelope plasmid pMD2.G (Addgene #12259) and expression plasmid (Addgene #19319). Briefly, HEK293T cells were seeded 24 h prior to transfection at a density of 400 K cells per well of a 6-well plate. 16 h after transfection with 800 ng psPAX2, 400 ng pMD2.G and 800 ng of expression plasmid with 6 µL X-tremeGENE 9 (Roche), medium was changed to 1.5 mL harvesting medium (DMEM + 10% FBS + 1.1 g/100 mL BSA) per well. 48 h after transfection, medium was collected and spun 3 min at 700 g to pellet residual cells. For transduction, 500 µL supernatant was added to one well of a 6-well plate with 300 K cells in 1.5 mL medium with 12 µg polybrene. After 24 h

incubation, medium was changed to fresh medium with 1 µg/mL Puromycin to select for successful integration. Cells were further enriched for high expression clones by FACS sorting based on the GFP signal. Cell lines were verified by measuring luciferase signal at different seeding densities to make sure that luciferase signal readout showed a linear correlation with cell numbers.

Generation of KP4 EPHA2 and EPHB2 knockout cell lines:

KP4 EPHA2 knockout cells were generated using CRISPR/Cas9 technology. Briefly, a gRNA sequence targeting exon3 of human EPHA2 or exon1 of human EPHB2 was cloned into a modified version of CRISPR/Cas9 vector pSpCas9(BB)-2A-Puro (PX459), a gift from Feng Zhang (Addgene plasmid # 62988),⁴⁴ which was transiently transfected into KP4 cells using Lipofectamine3000 (ThermoFisher #L3000001). Successfully transfected cells were enriched by selection in RPMI + 10% FBS + 2.5 µg/mL Puromycin for 24 h, then trypsinized and seeded in RPMI + 10% FBS into 96-well plates at concentrations of 0.5–1 cells per well. Wells were regularly inspected for colony growth and wells with single colonies were expanded further. Of the multiple cell lines that showed loss of EPHA2 or EPHB2 by Western blot, two were further confirmed to have lost surface display of EPHA2 and EPHB2, respectively, by flow cytometry. Both clones showed similar growth properties to KP4 parental cells. The EPHA2 KO line was confirmed to harbor frame-shift inducing InDels on both alleles of exon3 (+1/-110 nt) by Sanger sequencing of various PCR amplicons of exon3.

EPHA2 exon3 gRNA: GAACGTGGAGGAGCGCTCCG
EPHB2 exon1 gRNA: GCGCAGCCATGGCTCTGCGG

Cytotoxicity assays:

Tumor cell lines were seeded overnight into black, clear-bottom 96-well plates (Corning #3904) to achieve confluency the next day (seeding numbers: KP4 20,000–30,000 cells/well, HCT116 50,000 cells/well, RCC243 20,000 cells/well, GP5A 20,000 cells/well, GP13A, 14A, 16A 30,000–45,000 cells/well). The next day cells were treated with PBMCs (ATCC #PCS-800-011) at desired E:T ratios and DATES. Unless stated differently, 80,000–100,000 PBMCs were added per well, resulting in E:T ratios of 4:1–5:1 for KP4 cells, 4:1–5:1 for RCC243 cells and 2:1 for HCT116 cells. As far as possible, different PBMC lots representing different human donors were used for biological replicates of the same experiment. Endpoint viability assays were performed 3 d after treatment started. For cell lines stably expressing firefly luciferase, viability was assessed by measuring remaining luciferase activity in each well as previously described⁴⁵ using Bright-Glo luciferase substrate (Promega #E2650). For wild-type KP4, HCT116 and patient-derived cell lines, wells were gently rinsed with PBS to wash off PBMCs. The viability of the remaining cells was measured using CellTiter-Glo substrate (Promega #G7571). For both assays, medium or PBS, respectively, was removed and 40 µL PBS + 40 µL substrate added per well. Cell lysis was facilitated by orbital shaking for 2 min. Plates were incubated 10 min in the dark and luminescence signal acquired using an Epoch Synergy

(10 sec integration, 130 gain). Signal in each well was normalized to matching control wells that received the same amount of PBMCs but no DATEs (named “untreated” in figure legends; considered 100% viability) and data plotted ($\text{signal}_{\text{sample}}/\text{signal}_{\text{untreated}} \times 100$). For each experiment samples were run in technical duplicates or triplicates. N-numbers indicate biological replicates and error bars represent standard deviation.

Jurkat NFAT reporter assay:

Tumor cell lines were seeded overnight into 96-well plates to achieve confluent wells the next day (seeding numbers: KP4 30,000 cells/well, HCT116 60,000 cells/well, HEK293 WT or CD133-overexpressing 50,000 cells/well). The next-day medium was replaced with 50- μL complete RPMI medium (ATCC formulation), containing DATEs and 100,000 Jurkat NFAT-luc cells (BPS Bioscience # 60621) per well. After 24 h, NFAT reporter activation was assessed by measuring the remaining luciferase activity in each well using Bright-Glo luciferase substrate (Promega #E2650). Briefly, 50 μL substrate was added per well and cell lysis was facilitated by orbital shaking for 2 min. Plates were incubated 10 min in the dark and luminescence signal acquired using an Epoch Synergy (10 sec integration, 130 gain). Signal in each well was normalized to matching control wells that received the same amount of Jurkat cells but no DATEs (named “untreated” in figure legends; considered baseline) and data was plotted as signal/baseline ($\text{signal}_{\text{sample}}/\text{signal}_{\text{untreated}}$). For each experiment samples were run in technical duplicates or triplicates. N-numbers indicate biological replicates and error bars represent standard deviation.

Flow cytometric analysis of tumor cells and PBMCs:

Commercial and patient-derived tumor cell lines were detached using StemPro Accutase Cell Dissociation Reagent (ThermoFisher #A1110501) or 10 mM EDTA (Invitrogen #15575-038). After washing, cells were resuspended in FACS buffer (PBS containing 2% heat-inactivated FBS (Fisher Scientific #10-082-147) and 0.1% sodium azide (Biobasic #DB0613)) and plated at 2.5×10^5 cells/well of a 96-well round-bottom plate. Cells were stained with antibodies for 30 min on ice in a total volume of 100 μL FACS buffer. For quantification of EPHA2 and EPHB2 expression on tumor lines, primary staining was performed with 100 nM anti-EPHA2 or EPHB2 profiler Fabs. For CD133 expression, mouse antihuman CD133 IgG (Biolegend clone W6B3C1 # 397902) was used for primary staining at 1:250 dilution. EpCAM expression was quantified directly with APC/Fire 750-conjugated antihuman CD326 (Biolegend; Clone 9C4). For DATE or d-DATE titrations, primary staining was performed with antibody concentrations ranging from 0.01 to 1500 nM. Depending on the expression of GFP in cell lines, and other fluorochrome-conjugated antibodies in the panel, secondary staining of Fabs or DATEs was performed with either 1:500 Alexa Fluor 488-conjugated, 1:400 APC-conjugated, or 1:400 Alexa Fluor 647-conjugated Affinipure F(ab')₂ fragment-specific goat antihuman IgG (Jackson ImmunoResearch #109-545-097, #109-136-097, or #109-606-097), or 1:500 PE-conjugated rat anti-FLAG

antibody (Biolegend; Clone L5). PE-labeled goat anti-mouse IgG (Jackson ImmunoResearch #115-116-146) was used at 1:400 dilution for secondary detection of anti-human CD133 IgG. Fixable viability dyes eFluor 450, eFluor 455UV, or eFluor 780 (ThermoFisher #65-0863-14, #65-0868-14, or #65-0865-14) were used to exclude dead cells. Cells were acquired on a Cytoflex instrument or BD FACS Canto HTS, and results were analyzed with FlowJo software (BD Biosciences). Fluorescent signals were reported as the half log of the median fluorescence intensity (MFI) of a given sample normalized to the MFI of the secondary antibody alone ($\log_2(\text{MFI}/\text{MFI}_0)$).

For human PBMC staining, either for profiling of EPHA2 and EPHB2 expression or for the evaluation of T-cell activation by DATEs in the presence of tumor cells, cells were first blocked in 50 μL of brilliant staining buffer (BD Biosciences #566349) containing 5 μL human FcR blocking reagent (Miltenyi Biotec #130-059-901) and 3% normal mouse serum (Abcam #ab7486). Then 50 μL of brilliant staining buffer containing the following antihuman antibodies was added to label different PBMC subsets: BUV395 anti-CD4 (Clone SK3), BUV737 anti-CD56 (Clone NCAM16.2), V450 anti-CD45 (Clone HI30), BV510 anti-CD45RO (Clone UCHL1), APC anti-CD3, BB700 or APC-H7 anti-CD8 (Clones RPA-T8 and SK1), Biotinylated anti-CD19 and anti-CD33 (Clones HIB19 and WM53). T-cell activation was assessed with Super bright 600 anti-4-1BB (Clone 4B4), BV786 anti-CD25 (Clone M-A251), BB700 PD-1 (Clone EH12.1), and PE-Dazzle 594 anti-CD69 (Clone FN50). Secondary staining was performed for 30 mins in a total volume of 100 μL PBS containing APC-R700 streptavidin (BD Biosciences #565,144) and Fixable viability dye eFluor 455UV for T-cell activation, or PE-labeled anti-Flag, V450 streptavidin (BD Biosciences #560,797), and Fixable viability dye eFluor 780 for EPH expression. Cells were acquired with a BD FortessaTM X-20 instrument and FACSDiva software (BD Biosciences).

In vivo testing of DATEs in a PDAC xenograft model:

Immunodeficient male and female NSG-SGM3 mice (Jackson Laboratories, Bar Harbor, ME, USA; strain# 013062) were housed in a pathogen-free environment at the animal facility of the University of Toronto. The study was conducted according to the guidelines of the Canadian Council on Animal Care (CCAC) and the animal use protocols approved by the University Animal Care Committee (UACC) at the University of Toronto. At 9 weeks of age, animals were inoculated subcutaneously in their right flank with 4×10^6 KP4 cells, which were detached from the cell culture dish with Accutase, washed with complete RPMI medium and DPBS, and resuspended in 100 μL of a 1:1 mixture of PBS and cold Matrigel matrix (Corning #356237) for injection. Tumor volumes were measured using a Vernier caliper and calculated using the formula: $(\text{Length} \times \text{Width}^2) \times \pi/6$. Animal weights and tumor volumes were measured two times weekly from the start of tumor engraftment. One day before the start of DATE administrations, animals were assigned to experimental groups such that the average tumor volume in each group was about 300 mm^3 . An intravenous (i.v.) dose of 2 mg/kg DATE was injected the following day. 24 h later, 3×10^7 *in vitro*-expanded human T cells were adoptively transferred i.v. to the mice, and animals received additional i.v.

administrations of 2 or 4 mg/kg DATE 1 d and 6 d after T-cell transfer, respectively. Ten days before T-cell adoptive transfer, cryopreserved human PBMCs (ATCC #PCS-800-011) were thawed, washed and resuspended at about 1×10^6 cells/mL ImmunoCult-XF T-cell expansion medium (Stem Cell Technologies #10981) containing 1% penicillin-streptomycin. Cells were allowed to rest for 6 h before the addition of 25 μ L/mL ImmunoCult Human CD3/CD28 Activator (Stem Cell Technologies #10971) and 5 ng/mL recombinant human IL-2 (Peprotech #AF-200-02), IL-7 (Peprotech #AF-200-07) and IL-15 (Peprotech #AF-200-15). Suspended cells were then transferred into 6-well plates in order to seed the cells at 1×10^6 cells/mL/cm² and to remove adherent cells. Cells were divided on days 3, 5, and 7 and total medium volume was increased four-fold on days 3 and 5, and three-fold on day 7. Also, additional IL-2, IL-7 and IL-15 cytokine was added on each of these days, maintaining cytokine concentrations at 5 ng/mL and cell density between 1 and 2.5×10^5 cells/mL during their expansion. On day 10 of expansion, cells were collected in 500 mL sterile flasks, washed with 100 mL DPBS, and resuspended at 3×10^7 cells per 0.2 mL DPBS for i.v. injection into mice. Injected cells were confirmed by flow cytometry to be >96% CD3 + T cells (**Supplementary Figure S4A**). The ability of these cells to kill KP4 cells stably expressing firefly luciferase was also confirmed *in vitro* using the cytotoxicity assay described earlier (**Supplementary Figure S4B**).

Immunohistochemical staining of PDAC tumors:

Formalin-fixed, paraffin-embedded tissue sections were pre-treated with low-temperature Tris-EDTA (pH 9.0) and heat-induced epitope retrieval. Sections were stained with rabbit monoclonal anti-human CD3 Ab (Ventana; Clone 2 GV6) and visualized with MACH 4 Universal HRP-polymer detection kit (Biocare Medical #M4U534), using 3,3'-diaminobenzidine as the chromogen. Slides were scanned in brightfield at 20x magnification using the Aperio Scanscope AT2 instrument and images were generated using Aperio ImageScope software (Leica Biosystems, Wetzlar, Germany).

Statistical analysis

Data were analyzed using GraphPad Prism 7 (GraphPad Software, Inc., La Jolla, Calif.) and are presented as means \pm standard deviation. To evaluate significance, differences between groups of three or more were identified by analysis of variance (ANOVA). Tumor volumes were analyzed by regular two-way ANOVA and simple effects within rows (comparison of experimental groups at a given time point) were tested. A value of $P < 0.05$ was considered statistically significant.

Results

Design and construction of DATES and d-DATES

We sought to develop a modular T-cell redirection discovery platform to target pancreatic and other solid tumors using a toolbox of synthetic antibodies, which enables facile assembly of T-cell redirection modalities. Focusing on tumor-initiating

populations thought to potentiate resistance and metastasis, we developed antibodies (**Figure 2a**) against the TIC markers CD133 and EPCAM, and the receptor tyrosine kinase (RTK) EPHA2, which have been used previously as TAAs for T-cell redirection or CAR-T therapies^{46–51} (clinical trials NCT03013712, NCT02541370). We intended to use paratopes against EPCAM (named EC-1), EPHA2 (named A2-1, A2-2, A2-3, A2-4) and CD133 (named 133–1) as primary agents (“killing arm”), and thus, we developed antibodies against these antigens in the Fab format using a validated, phage-displayed synthetic Fab library built on the trastuzumab framework.³⁸ We also targeted the RTK EPHB2, which we found frequently co-expressed with EPHA2 in pancreatic cancer cells (see below), with a paratope that would act as a secondary targeting agent (“auxiliary arm”). Thus, we developed an antibody against EPHB2 in the autonomous VH domain format (named B2-1), using phage-displayed human VH domain libraries built with an autonomous framework, also derived from trastuzumab.⁵² Finally, to enable T-cell recruitment, we humanized the validated murine anti-CD3 OKT3 muromonab antibody by grafting the complementarity-determining region (CDR) loops into the trastuzumab framework in a scFv format (humanized OKT3 herein named hOKT3) (**Supplementary Figure S1**). Affinity measurements of these antibodies to their cognate antigens revealed low to sub-nanomolar binding constants (**Figure 2b**). Moreover, we observed high selectivity of the anti-EPHA2 and anti-EPHB2 antibodies for their respective antigens relative to the entire set of 14 human EPH receptors (**Figure 2c**). Thus, using phage display and humanization methods, we were able to develop selective and potent antibodies in appropriate formats for modular assembly of recombinant T-cell redirection modalities.

In contrast to classical BiTE formats that consist of two scFvs fused in tandem, the DATE format contains a Fab fused to a scFv. Incorporating a Fab ensures VH/VL fidelity through a covalent disulfide link between the heavy and light chain. To assemble DATES, the hOKT3 scFv was attached C-terminally to the anti-TAA Fab light chain (**Figure 1**). In this design, the Fab heavy and light chains form a stable covalent complex and any potential for intramolecular exchange with the VH and VL domains of the fused scFv are obviated. Using our toolbox of antibodies (**Figure 2**), we used this format to create a panel of DATES targeting EPHA2, EPCAM, and CD133, as well as Gaussia luciferase (named GLuc), which is not expressed in mammalian cells, as a negative control. For targeting EPHA2, we developed DATES with Fabs of four different paratopes (A2-1, A2-2, A2-3, A2-4) since competition assays showed that each Fab recognized an epitope distinct from those of the others (**Supplementary Figure S2A**). We showed that each DATE recognized its cognate antigen by ELISA with recombinant proteins (**Figure 2d**, **Supplementary Figure S2B**) or by flow cytometry with tumor cell lines (**Figure 2e–g**). Size-exclusion chromatography (SEC) showed predominantly homogeneous monodispersed behavior for DATES generated from Fabs with similar properties (**Supplementary Figure S2C**). We also generated DATES where the anti-CD3 scFv contained a murine framework (herein referred to as mOKT3) based on the BiTE molecule blinatumomab (**Supplementary Figure S1**). Notably, we observed that the yield and homogeneity of DATE proteins containing hOKT3 scFv were substantially improved over those containing mOKT3 scFv, which facilitated the

SDS-PAGE showed that, under nonreducing conditions, each d-DATE protein ran predominantly as a single band that migrated at a size consistent with a covalently linked assembly of the two chains, and under reducing conditions, as two bands that migrated at sizes consistent with those of the two separate chains (Figure 3b). Similar to their parental A2-4 DATE, by SEC, d-DATES with the VH domain fused to the N- or C-terminus of the Fab heavy chain eluted primarily as a single peak indicative of monodispersed behavior (75% and 90% of total protein, respectively) with a small shoulder indicative of a small percentage of aggregation or oligomerization. Furthermore, d-DATES could be purified to 95% purity by preparative SEC (Figure 3c-d). Finally, we confirmed by ELISA that N- and C-terminally fused d-DATES recognized both EPHA2 and EPHB2 (Figure 3d). The introduction of longer linkers between the Fab and VH domain did not affect the biophysical properties (Figure 3a-b). Taken together, these results showed that functionally complex d-DATES with favorable production characteristics and improved homogeneity based on hydrodynamic volume can be assembled in a facile manner using mutually compatible modular scFv, Fab and VH domains for recognition of CD3 and the first and second TAA, respectively.

Assessment of DATE specificity and efficacy

To establish solid tumor cell models to evaluate DATE cytotoxicity, we focused on pancreatic ductal adenocarcinoma (PDAC). To this end, we quantified the surface display of TAAs *in situ* in both commercial (KP4) and patient-derived (GP5A, GP13A, GP14A, GP16A) pancreatic tumor lines and selected cell lines with a differential display of EPCAM, CD133, EPHA2, and EPHB2 (Figure 4a). All pancreatic lines displayed high levels of EPHA2 and lower levels of EPHB2. EPCAM was displayed at high levels in all GP lines, but was low in KP4 cells. GP13A additionally displayed CD133, whereas KP4 and the other GP lines did not. As additional solid tumor models, we used the colon cancer line HCT116, which displayed all four TAAs, and the renal clear-cell carcinoma line RCC243, which displayed EPCAM, EPHA2 and low levels of EPHB2, but not CD133 (Figure 4a). We also screened other solid tumor cell lines for endogenous expression of the stem cell marker CD133 by Western blot. We used a stable CD133 overexpression HEK293T cell line as a positive control and confirmed that the colon cancer line HCT116 was positive for CD133, comparable to the human embryonic stem cell line H1 (Figure 4b).

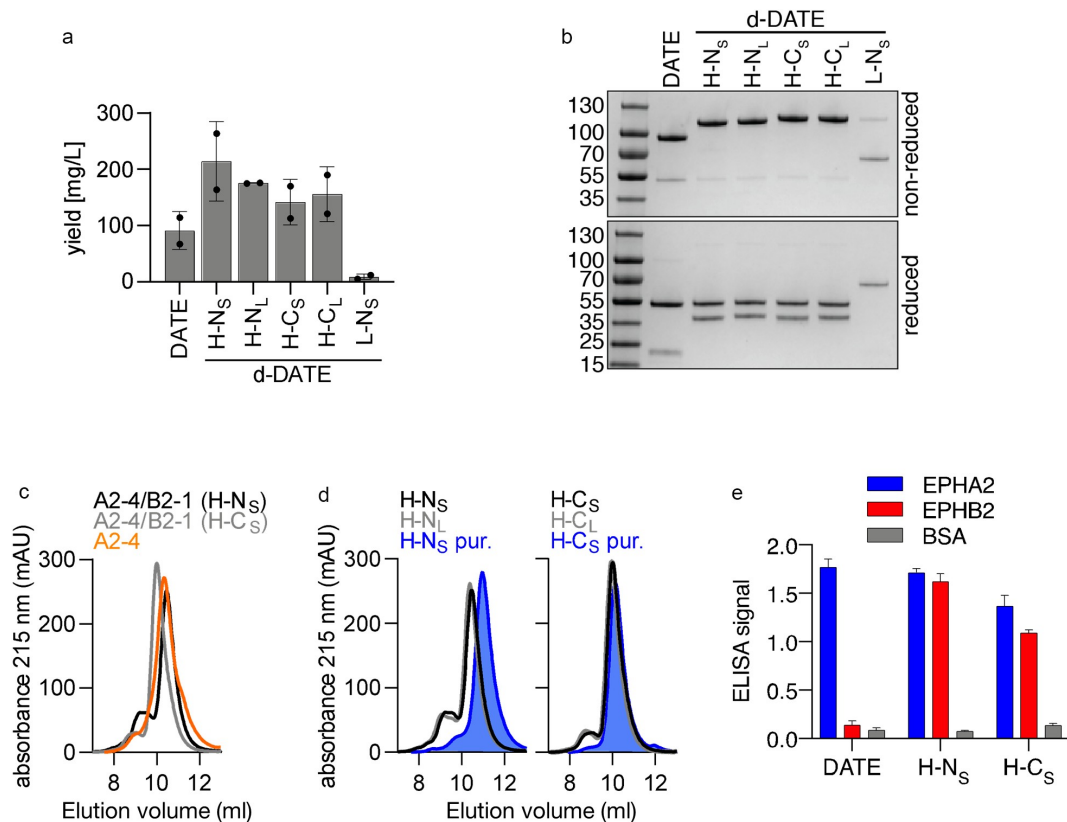


Figure 3. Characterization of d-DATES. Data are shown for d-DATES that contained anti-EPHA2 Fab A2-4 with hOKT3 scFv fused to the C-terminus of the light chain, and the anti-EPHB2 VH domain B2-1 fused to the N-terminus of the heavy chain (H-N_S and H-N_L), the C-terminus of the heavy chain (H-C_S and H-C_L) or the N-terminus of the light chain (L-N_S). Subscript "S" and "L" refer to short or longer linkers, respectively, connecting the VH domain to the Fab. **(A)** Yields of purified DATE and d-DATE proteins produced from Expi293 cells by transient transfection in 10 mL cultures ($n = 2$). **(B)** SDS-PAGE analysis of purified proteins under nonreducing (*top*) or reducing (*bottom*) conditions. Protein samples were heated in the absence (non-reduced) or presence (reduced) of 5% BME, electrophoresed, and stained with Coomassie blue (representative gel of $n = 2$). **(C)** Size-exclusion chromatography of d-DATES and their parental DATE. Chromatograms are shown for 1 mg/mL samples applied on a Tosoh TSKgel BioAssist G3SWxl column (column volume = 12 mL). **(D)** Size-exclusion chromatography comparison of d-DATE formats. Chromatograms are shown for 1 mg/mL samples of H-N (left) or H-C (right) formats applied on a Tosoh TSKgel BioAssist G3SWxl column (column volume = 12 mL). The following percentages of the total peak areas were determined for the main monomer peak: H-N_S, 75%; H-N_L, 76%; H-C_S, 90%; H-C_L, 89%. After monomer purification by size-exclusion chromatography of H-N_S and H-C_S, monomer homogeneity could be increased to 95% (H-N_S pur.) and 94% (H-C_S pur.) as depicted by the filled blue curves. **(E)** Assessment of specificity by ELISA. Signals (*y*-axis) were measured for 50 nM DATE or d-DATES (*x*-axis) binding to immobilized Fc-tagged EPHA2 or EPHB2 ECD or BSA (negative control). Data shown are averaged from two replicate wells. All error bars represent standard deviation about the mean.

Together, these cell lines formed a panel to assess synthetic DATE specificity and activity.

We first characterized DATE functionality on human T cells. DATE-mediated activation of the T-cell receptor (TCR) was verified in Jurkat reporter cells 24 h after co-culture with cancer cells, by measuring activation of a luciferase reporter under the control of the promoter for the nuclear factor of activator T cells (NFAT) gene. As expected, the Jurkat NFAT reporter was strongly activated by the 133-1 DATE specifically when co-cultured with HEK293T cells that overexpress CD133 (Figure 4c). Similarly, when co-cultured with KP4 cells, the reporter was specifically activated by EPHA2-targeting DATES, but not by DATES targeting EPCAM or GLuc, which are not expressed on KP4 cells (Figure 4d). TCR activation promotes the rapid upregulation of cell-surface activation markers in T cells. Therefore, T-cell activation markers were quantified by flow cytometry in peripheral blood mononuclear cells (PBMCs) after 48 h of co-culture with KP4 cells and DATES. Induction of the early activation markers CD69, PD-1, and CD25 was confirmed based on the increased frequency of CD4⁺ and CD8⁺ T cells expressing these markers after PBMC culture with EPHA2-targeting DATES, but not with the LUC-1 control DATE (Figure 4e, Supplementary Figure S3A). Furthermore, the frequency of CD8⁺ T cells expressing the inducible costimulatory molecule 4-1BB was significantly elevated by EPHA2-targeting DATES only. Human interferon- γ (IFN- γ) was measured in supernatants after 3 d of tumor cell culture with PBMCs and was specifically induced by three out of the four EPHA2 DATES that were tested, but not by the LUC-1 DATE (Supplementary Figure S3B). These results indicated that T-cell activation by a DATE occurs only in the presence of cancer cells that display the specific antigen targeted by the Fab module of the DATE.

Next, we evaluated if DATES could elicit a cytotoxic response from T cells by treating monolayers of tumor cells with donor PBMCs and DATES, and then assessing tumor cell viability after 3 d. One of two assays was used to detect the percentage of remaining live tumor cells at the endpoint, depending on whether the cells expressed firefly luciferase. We generated KP4, HCT116 and RCC243 cell lines stably expressing firefly luciferase, which enabled the measurement of target cell viability without interference from PBMCs. At the endpoint, after addition of luciferase substrate, the luminescence readout correlates with the number of viable tumor cells (luciferase assay⁴⁵). For all other cell types, we performed ATP-dependent luminescence-based CellTiter-Glo assays, after rinsing the target cells to remove contaminating PBMCs. By quantifying cell viability at endpoint with these methods, we found that the DATES promoted potent cytotoxicity in cell lines displaying their cognate TAA, but not in cells with no or low antigen display. All EPHA2-targeting DATES induced strong cytotoxicity on KP4, HCT116, GP5A and GP13A lines, while EC-1 DATE was only effective in the EPCAM-displaying lines HCT116, GP5A and GP13A. The 133-1 DATE specifically killed HCT116 and GP13A, but not KP4 or GP5A cells (figure 4f). The negative control LUC-1 DATE had no effect on any cell line (figure 4f, Supplementary Figure S3F-I). Importantly, the cytotoxic response was T cell-dependent,

where maximum cytotoxicity in KP4 cells was reached at a 4:1 effector (E) to target (T) cell (E:T) ratio (Supplementary Figure S3C), and no effect of DATES on cell viability was observed in the absence of PBMCs (Supplementary Figure S3D-F). To quantify the effective concentrations of each DATE, we titrated 133-1 and EC-1 DATES on HCT116 cells and EPHA2-targeting DATES on KP4 cells, while keeping the E:T ratio constant (Figure 4g, Supplementary Figure S3F-G). The extent of cytotoxicity was dose-dependent, ranking with the affinity of the DATE for the TAA, and all DATES were extremely potent with low to subnanomolar EC50s. Finally, we evaluated the broader application of our DATES across the panel of patient-derived pancreatic cell lines (GP5A, GP13A, GP14A, GP16A) and RCC243 cells (Supplementary Figure S3G-I). We observed *in vitro* DATE-mediated cytotoxicity in each cell line displaying the relevant TAA, albeit to varying degrees. Together, these data demonstrate a robust application of DATE modalities to induce targeted T-cell cytotoxicity *in vitro* in multiple solid tumor cell models by targeting three different TAAs.

We also confirmed DATE activity *in vivo*, using a mouse xenograft model of KP4 PDAC, which displays high levels of EPHA2. We tested the two most potent anti-EPHA2 DATES from *in vitro* cytotoxicity assays that recognized both human and mouse EPHA2 (A2-1 and A2-2) (Figure 2d). T cells were expanded from human PBMCs and tested *in vitro* with EPHA2-targeting DATES and KP4 cells (Supplementary Figure S4A-B). Expanded T cells were effective in killing tumor cells and were more potent than PBMCs used in equivalent assays. We also demonstrated that CD4⁺ and CD8⁺ T cells are low in EPHA2 display, suggesting that binding of the DATES to T cells is mainly mediated through the hOKT3-CD3 interaction (Supplementary Figure S4C). For the *in vivo* study, DATES were administered to NSG-SGM3 mice, which lack mature T cells, bearing KP4 tumors with a volume of ~300 mm³. Expanded human T cells were adoptively transferred the following day, and animals subsequently received two additional DATE administrations and tumor size was monitored for 2 weeks (Figure 5). Tumor-infiltrating human CD3 + T cells were detected by immunohistochemical analysis in resected tumors at endpoint (Supplementary Figure S4D). Consistent with our *in vitro* data, a significant reduction of tumor growth was observed in mice treated with the A2-1 and A2-2 DATES, compared to animals treated with the negative control LUC-1 DATE. In sum, these data demonstrate that EPHA2-targeting DATES can drive efficacious T-cell responses in solid tumor models.

Assessment of d-DATE specificity and activity

A major challenge for immunotherapies targeting overexpressed cancer antigens is toxicity through the recognition of healthy cells with shared target expression. We reasoned that addition of an antibody fragment targeting a second TAA to our DATE format would enhance cell and tissue selectivity, beyond what could be achieved by DATES targeting a single TAA. EPHA2 overexpression is a common feature of pancreatic carcinoma,^{53,54} while less is known about co-expression patterns with other members of the EPH receptor family,

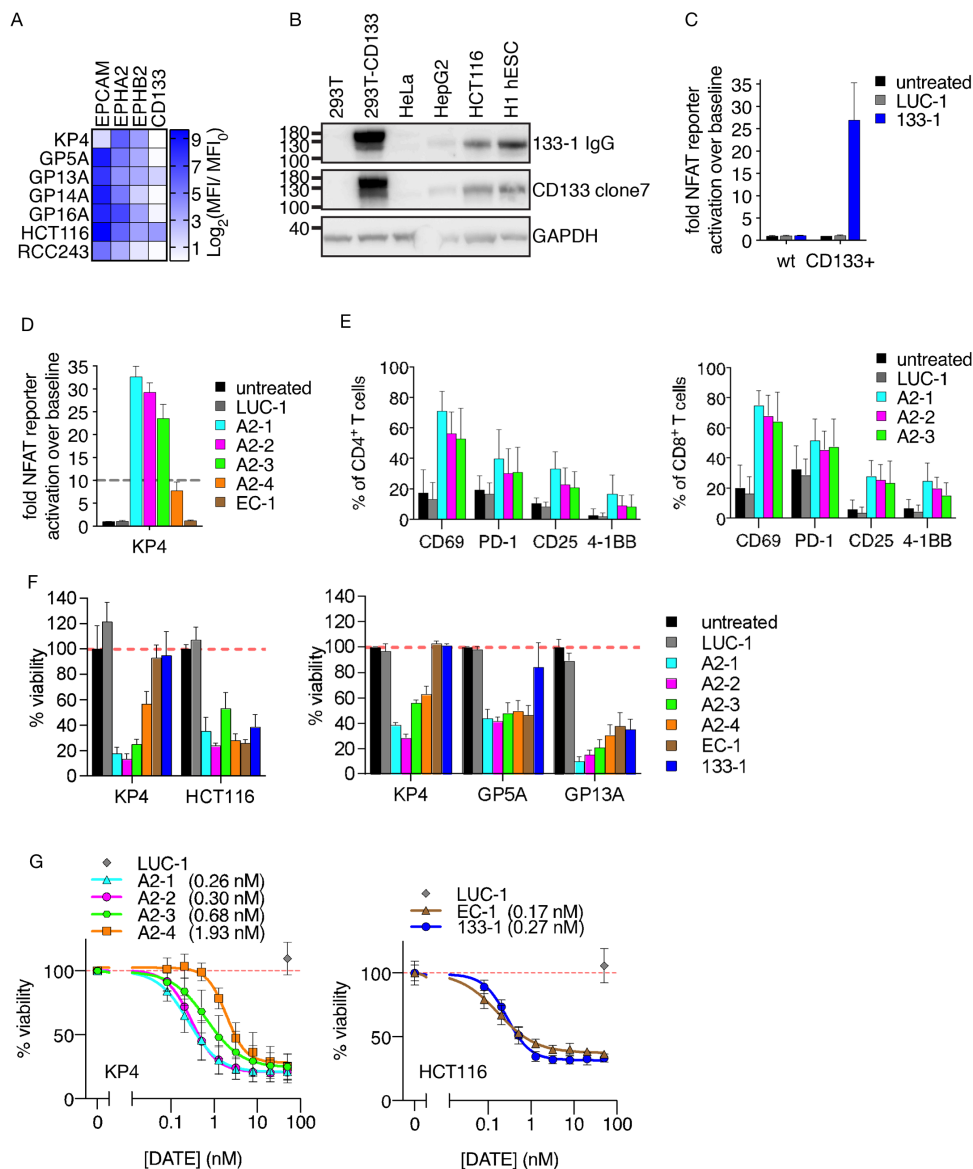


Figure 4. Cytotoxic effects of DATEs on tumor cell lines. **(A)** Display of antigens (x-axis) on cancer cell lines (y-axis), assessed by flow cytometry. Binding signal normalized to samples stained with secondary antibody only (data pooled from $n = 3$ independent experiments, each with technical replicates). **(B)** Western blot of whole-cell lysates probed with 133-1 IgG or commercial anti-CD133 clone7 (Biolegend #372,802) and GAPDH as the loading control. CD133 is strongly expressed in CD133 overexpressing HEK293T cells, HCT116 cells, and H1 human embryonic stem cells (hESC). **(C)** Jurkat NFAT reporter activation in response to DATEs after 1 day of co-culture with CD133-negative (WT) or CD133 overexpressing (CD133+) HEK293T cells. (5 nM DATEs, NFAT-luc assay) ($n = 2, 3$ technical replicates each). **(D)** Jurkat NFAT reporter activation in response to DATEs after 1 day of co-culture with KP4 cells. (5 nM DATEs, NFAT-luc assay) ($n = 2, 2$ technical replicates each). Dashed line indicates 10-fold over baseline. **(E)** Frequency of CD4⁺ (left) and CD8⁺ (right) T cells (y-axis) displaying activation markers (x-axis) after co-culture for 48 h with KP4 cells in the presence of 5 nM of each indicated DATE (data pooled from $n = 3$ independent experiments with PBMCs from a total of 9 different donors). **(F)** Viability (y-axis) of cancer cell lines (x-axis) assessed by luciferase expression (left, 0.5 nM DATEs) ($n = 2, 3$ technical replicates each) or CellTiter-Glo assay (right, 50 nM DATEs) ($n = 2, 2$ technical replicates each) following treatment with DATEs and PBMCs for 3 d. **(G)** Dose–response curves for viability (y-axis) of indicated cancer cell lines treated for 3 d with serial dilutions (x-axis) of DATE (0.08 nM – 50 nM) containing the indicated anti-tumor antigen Fab, in the presence of PBMCs. Cell viability was determined by luciferase expression at endpoint ($n = 3, 2$ technical replicates each). All error bars represent standard deviation about the mean.

which comprises 14 members. EPH receptors form homomeric and heteromeric clusters,⁵⁵ and we explored whether EPHB2 was upregulated along with EPHA2 in PDAC cell lines. We used highly specific Fabs and flow cytometry to profile cell-surface levels of EPHA2 and EPHB2 on KP4 and various patient-derived pancreatic cell lines. We consistently found EPHA2 to be displayed highest and that EPHB2 was generally highly co-displayed with EPHA2 (Figure 4a). Whereas RCC243 cells showed lower EPHB2 surface display, a similar pattern was found in HCT116 cells. We therefore selected

EPHA2 and EPHB2 to develop and validate the novel d-DATE modality for targeting co-expressed tumor antigens. To this end, we fused an EPHB2-targeting VH domain to our EPHA2-targeting DATEs to yield EPHA2/EPHB2 co-targeting d-DATEs (Figure 1b).

We started with the less efficacious and lower affinity A2-4 DATE as a basis to generate d-DATEs, in order to facilitate the detection of potentially increased binding or killing after the addition of the VH domain. We fused the B2-1 VH domain to the N- or C-terminus of the Fab in the A2-4 DATE with short

(S) or long (L) linkers (named H-N_{S/L}-A2-4/B2-1 and H-C_{S/L}-A2-4/B2-1, respectively) and tested the ability of these d-DATEs to activate TCR signaling in Jurkat NFAT reporter cells (**Supplementary Figure S5A-B**). All four d-DATEs promoted TCR activation in this cell line in a dose-dependent manner when co-cultured with KP4 and HCT116 cells. Constructs with short and long linkers behaved similarly, but activation was greater with d-DATEs that contained the B2-1 VH domain fused to the N-terminus rather than the C-terminus of the A2-4 Fab heavy chain, implying that C-terminal fusions have an unfavorable domain geometry for T-cell activation (**Supplementary Figure S5A-B**). We focused on d-DATEs with short linkers and tested their cytotoxic activity in H-N_S and H-C_S formats on various target cell lines. We observed cytotoxicity for both formats on luciferase-expressing KP4 cells, but in accordance with Jurkat activation data, we found that H-N_S-A2-4/B2-1 clearly outperformed H-C_S-A2-4/B2-1, and also outperformed the A2-4 DATE (**Figure 6a**). Consistent with avidity effects from co-targeting of EPHA2 and EPHB2, both d-DATEs bound to KP4 cells with higher apparent affinities compared to their DATE counterpart. Moreover, consistent with relative cytotoxicity, H-N_S-A2-4/B2-1 exhibited the highest relative binding affinity (**Figure 6b**). We further evaluated the cytotoxic activity of the d-DATEs on HCT116 cells and patient-derived pancreatic cells; the effect of d-DATEs was equivalent to that of the A2-4 DATE, indicating that the VH domain neither enhanced nor compromised the cytotoxic activity of this T-cell engager in these cell lines (**Figure 6c-d**). In all experiments, we observed no effects on cell viability in the absence of PBMCs (**Supplementary Figure S5C-D**).

As an additional control we also generated an A2-4 d-DATE in the H-N_S format in which the VH domain contained a nonbinding (NB) paratope containing the LUC-1 CDRs (referred to as A2-4/NB) (**Supplementary Figure S5E**). We

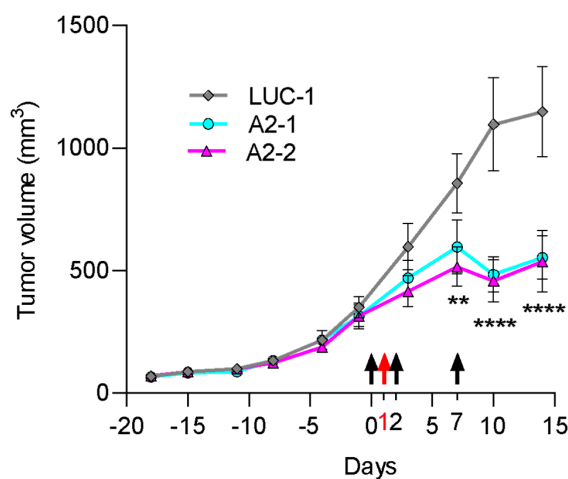


Figure 5. Effects of anti-EPHA2 DATEs in the subcutaneous KP4 xenograft model. NSG-SGM3 mice received an intravenous dose of 2 mg/kg of the indicated DATE upon tumors reaching an average volume of 300 mm³ within the cohort. One day later, 3×10^7 *in vitro*-expanded human T cells were adoptively transferred to the mice. One day and 6 d after T-cell transfer, the mice received additional administration of 2 or 4 mg/kg DATE, respectively. Black and red arrows indicate DATE administration or T-cell transfer, respectively. Tumor volume was monitored by caliper measurements ($n = 8$ –10 mice/group pooled from two independent experiments; ** $p < .01$, **** $p < .0001$).

directly compared binding strength and cytotoxic ability of A2-4 DATE, A2-4/NB d-DATE and A2-4/B2-1 d-DATE on KP4 cells (**Supplementary Figure S5F-H**). In cytotoxicity assays, we corroborated our findings using both wild type (WT) and luciferase-expressing KP4 cells for a direct comparison of the CellTiter-Glo and luciferase assays, respectively (**Supplementary Figure S5G-H**). Both assays gave qualitatively similar results, but consistent with previous experiments, the luciferase assay showed higher sensitivity due to the direct readout of cancer target cells without confounding signals from PBMCs. We found that the addition of the NB VH domain reduced binding and cytotoxicity of the A2-4 d-DATE to a degree, indicating some interference with Fab target binding. However, in comparison, binding strength and cytotoxicity were enhanced >20 fold when the NB VH domain was replaced with the B2-1 VH domain (**Supplementary Figure S5F-H**). Therefore, in KP4 cells specifically, the engagement of EPHB2 as a second antigen by the A2-4/B2-1 d-DATE can enhance the affinity of this T-cell engager toward its target cell and even augment its cytotoxic activity. These data demonstrate that additional arming of the DATE format with a second binding site can produce d-DATEs with the capacity to engage two TAAs on a target cell with potentially enhanced activity.

Uncoupling target engagement from T-cell cytotoxicity

In order to better understand how the VH domain influences DATE targeting and activity, we generated the EPHB2 co-targeting d-DATE equivalents of all EPHA2, EPCAM and GLuc-targeting DATEs by fusing the B2-1 VH domain in the H-N_S orientation and confirmed that they were able to bind both targets by ELISA (**Figure 2d**). We tested DATEs and d-DATEs side-by-side for cytotoxicity with KP4 (medium EPHB2), HCT116 (medium EPHB2), and RCC243 (low EPHB2) cells. All d-DATEs showed similar efficacy as their respective DATEs at 5 nM (**Figure 7a**). A significant enhancement of cytotoxic activity, as shown for the A2-4/B2-1 d-DATE on KP4 cells (**Figure 6a**, **Supplementary Figure S5G-H**), was not observed for other molecules, and in the case of the EC-1 d-DATE, even a slight decrease in cytotoxic potency on HCT116 cells was detected (**Supplementary Figure S6A**). This suggests that the functional behavior of a d-DATE is influenced by the combination of TAAs and epitopes targeted, as well as the affinity of each paratope. Notably however, the B2-1 VH domain did not confer cytotoxicity by itself, as EC-1 d-DATEs equipped with the EPHB2-targeting arm remained unable to kill KP4 cells (EPCAM negative, EPHB2 positive), and the LUC-1/B2-1 d-DATE showed no efficacy in any EPHB2 positive cell line (**Figure 7a**).

To gain further insight into the mechanism of d-DATEs, we established KP4 cells lacking EPHA2 or EPHB2 display, using CRISPR/Cas9 genome editing. From multiple clonal lines that had lost EPHA2 or EPHB2, as evidenced by Western blot analysis, we selected a clone each with similar growth properties as the parental WT KP4 cells and confirmed loss of surface display by flow cytometry (**Figure 7b**, **Supplementary Figure S6B**). Flow cytometric analysis over a range of concentrations further revealed that, as expected, the EPHA2-targeting DATEs

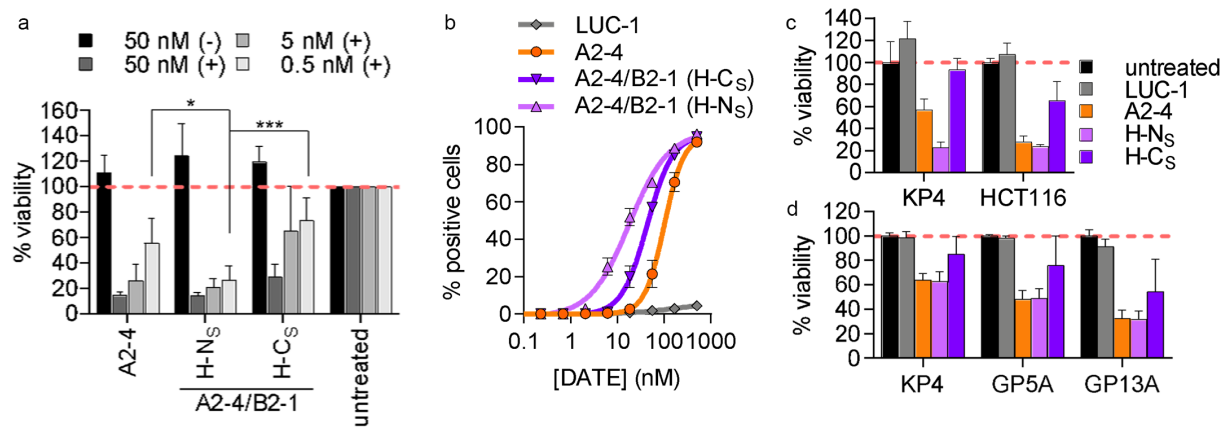


Figure 6. Functional characterization of d-DATE formats. **(A)** Viability of KP4 cells assessed by luciferase expression 3 d after treatment with the indicated concentration of the A2-4 DATE or the indicated A2-4/B2-1 d-DATE, in the presence (+) or absence (-) of PBMCs ($n = 4$, 3 technical replicates each; two-way ANOVA $*p < .05$, $***p < .0005$). **(B)** Dose–response curves for DATE or d-DATEs binding to KP4 cells assessed by flow cytometry ($n = 1$, 2 technical replicates). **(C)** Viability (y-axis) of cancer cell lines (x-axis) assessed by luciferase expression 3 d after treatment with 0.5 nM of the indicated DATE or d-DATE in the presence of PBMCs ($n = 2$, 3 technical replicates each). **(D)** Viability (y-axis) of cancer cell lines (x-axis) assessed by CellTiter-Glo assay 3 d after treatment with 50 nM of the indicated DATE or d-DATE in the presence of PBMCs ($n = 4$, 2 technical replicates each). All error bars represent standard deviation about the mean.

lost binding to EPHA2 knockout (KO) cells, but not EPHB2 KO cells (Figure 7c-d, Supplementary Figure S6C). In contrast, d-DATEs were consistently able to bind EPHA2 KO cells, indicating that the EPHB2-targeting VH domain can drive a high affinity cell interaction in the absence of binding through the EPHA2-targeting Fab. Similar to the observations with the A2-4/NB d-DATE (Supplementary Figure S5F), we also found a decrease in affinity of the EPHA2-targeting Fab in the presence of the VH domain when comparing binding of DATEs and d-DATEs on EPHB2 KO cells (where the VH domain is unable to bind). In contrast, binding of d-DATEs to WT cells relative to EPHB2 KO cells was enhanced in all cases, indicating avid binding in the presence of both TAA targets (Figure 7c-d, Supplementary Figure S6C). Therefore, although d-DATEs A2-1 to A2-3 did not show enhanced binding compared to their respective DATEs, they exhibited a subtle increase in selectivity toward dual antigen-expressing cells. The only d-DATE that displayed significantly enhanced affinity for WT cells was A2-4/B2-1, in which the EPHA2-targeting Fab is significantly weaker than the B2-1 VH domain (Figure 7c-d, Supplementary Figure S6C). Taken together, these data indicate that the EPHB2-targeting VH domain can enhance the selectivity of a d-DATE for cells that express both EPHA2 and EPHB2, as opposed to EPHA2 or EPHB2 alone, and significantly augments affinity toward dual-expressing cells when the VH is coupled with a lower affinity Fab.

Another important finding is that, when assayed in cytotoxicity assays, none of the d-DATEs were able to kill KP4 EPHA2 KO cells (Figure 7e) even though they bound these cells efficiently due to the EPHB2-targeting VH domain (Figure 7c-d). Consistent with this, we observed TCR activation only when Jurkat cells (NFAT reporter) were co-cultured in the presence of KP4 parental (WT) cells but not in the presence of EPHA2 KO cells (figure 7f). Moreover, DATEs and d-DATEs induced strong TCR activation on EPHB2 KO cells, at comparable levels to KP4 parental cells (Supplementary Figure S6D). Therefore, our anti-EPHB2 VH auxiliary arm has the capacity to augment binding

(especially when combined with a lower affinity Fab), but it cannot induce killing on its own. In contrast, the Fab killing arm mediates both binding and cytotoxicity.

To better understand why the B2-1 VH domain was unable to mediate killing by itself, we explored whether EPHB2, and the epitope bound by the B2-1 paratope in particular, was a suitable target for DATE-mediated killing. To this end, we generated EPHB2-targeting Fabs (Figure 2a) and converted them into DATEs, which we screened by biolayer interferometry (BLI) for competition with the B2-1 VH domain for binding to EPHB2 (Supplementary Figure S7). We identified two DATEs (B2-2 and B2-3) that competed with B2-1, and a third (B2-4) that did not. Like the B2-1 VH domain, B2-2 and B2-3 DATEs, but not B2-4, also competed with an Fc-tagged version of the natural ligand Ephrin B2 for binding to EPHB2, indicating that they bind to the ligand-binding domain of EPHB2 (Supplementary Figure S7).

To assess the activity of B2-2 and B2-3 DATEs, we tested their ability to bind KP4 cells and redirect and stimulate T cells. Both DATEs bound to KP4 cells with sub-nanomolar EC_{50} values (Figure 8a) and induced TCR activation (Jurkat NFAT reporter) on parental KP4 cells and EPHA2 KO cells, but not on EPHB2 KO cells (Figure 8b), thus demonstrating their specificity. Both DATEs also induced killing of KP4 cells when co-cultured with PBMCs (Figure 8c). These results showed that the B2-1 epitope is permissive for DATE-mediated cytotoxicity and that the inability of the B2-1 VH domain to induce killing in the auxiliary arm format must be due to other factors, such as geometry and/or distance relative to the T-cell recruitment arm. Taken together, our results support a mechanism in which d-DATEs can be designed to recognize cells expressing only the auxiliary arm TAA, but can only kill cells that co-display the killing arm TAA (Figure 9).

Discussion

In this study we characterized a DATE format that facilitates redirection of T cells to elicit cytotoxic effects on tumor cells,

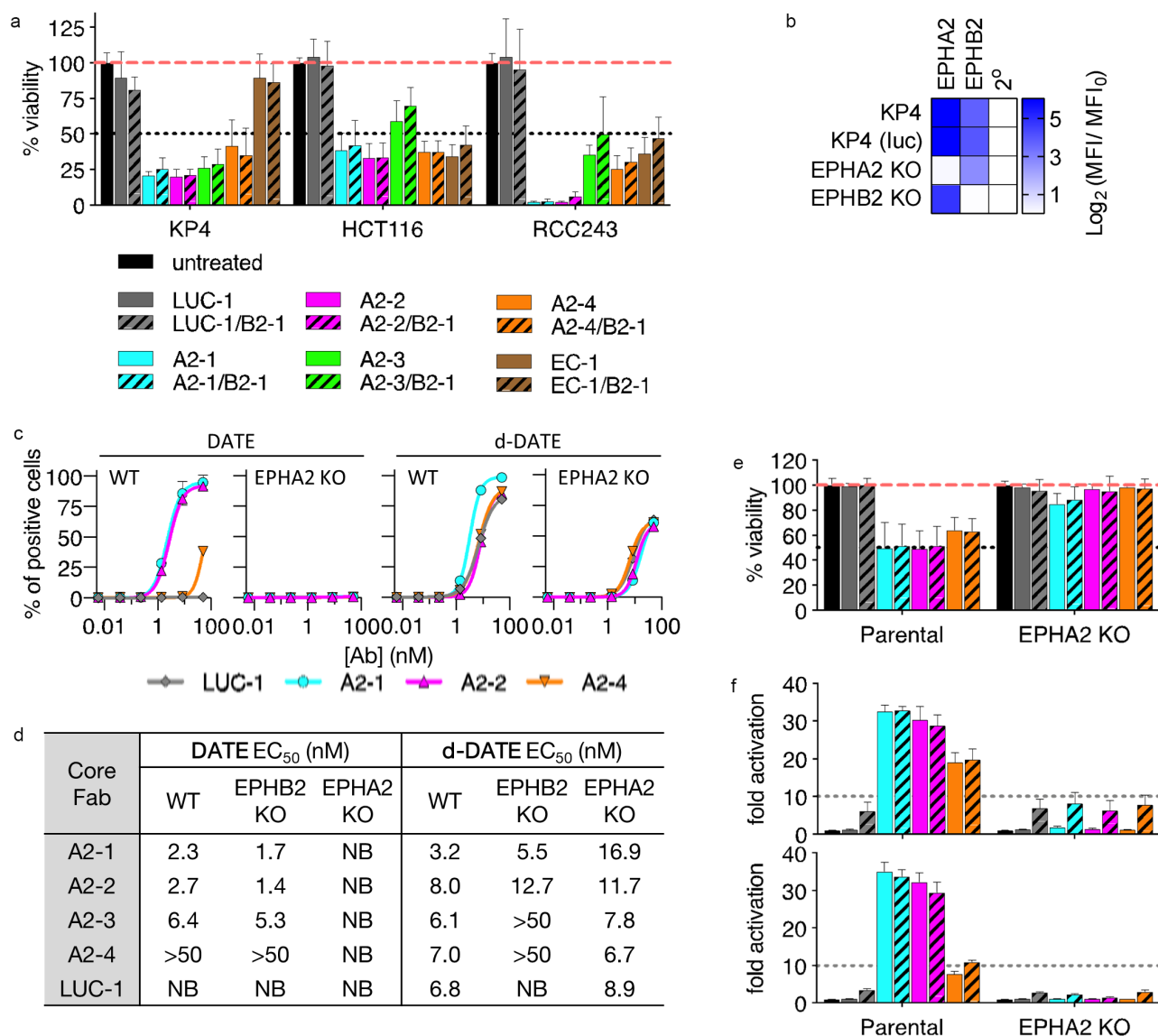


Figure 7. Cytotoxic effects of d-DATES on tumor cell lines. **(A)** Viability of luciferase-expressing KP4, HCT116, or RCC243 cells, assessed by luciferase expression 3 d after treatment with 5 nM DATES or d-DATES in the presence of PBMCs ($n = 3$, 2 technical replicates). d-DATES (striped) have similar cytotoxic effects as DATES (solid), and killing depends on the availability of the Fab target. Red and black dashed lines indicate 100% and 50% viability, respectively. **(B)** Flow cytometry profiling of EPHA2 and EPHB2 expression in KP4 parental, luciferase-expressing, EPHA2 KO, and EPHB2 KO lines ($n = 1$; 2 technical replicates). **(C)** Binding of DATES or d-DATES (all containing B2-1 VH domain) to KP4 parental (WT) and EPHA2 KO cells assessed by flow cytometry at various concentrations (0.006–50 nM) ($n = 1$; 2 technical replicates). **(D)** Comparison of DATES and d-DATES binding to cells. EC₅₀ values of DATES and d-DATES binding to KP4 parental (WT), EPHA2 KO, and EPHB2 KO cells as assessed by flow cytometry. Each row indicates molecules sharing the same core Fab. All d-DATES contain the B2-1 VH domain in H-N₅ format. NB = no binding. Complete set of graphs in Supplementary Figure S6F. **(E)** Viability of KP4 parental and KP4 EPHA2 KO cells assessed by CellTiter-Glo assay 3 d after treatment with 50 nM DATES or d-DATES in the presence of PBMCs ($n = 4$, 2 technical replicates each). Legend as in (A). Red and black dashed lines indicate 100% and 50% viability, respectively. **(F)** Jurkat TCR activation assessed by NFAT reporter assay 1 day after treatment of KP4 parental or EPHA2 KO cells with 50 nM (top) or 5 nM (bottom) DATES or d-DATES ($n = 2$, 2 technical replicates each). Legend as in (A). Gray dashed lines indicate 10-fold activation over baseline. All error bars represent standard deviation about the mean.

in vitro and *in vivo*. When directed toward appropriate epitopes, DATES are extremely potent T cell redirecting molecules that can be used to target and kill diverse cancer cell lines, including PDAC lines derived from patients. By using anti-tumor Fabs with a common, highly stable human framework, coupled to an anti-CD3 scFv with the same framework, we reliably purified many distinct DATES with protein yields comparable to those of full-length IgG molecules. Furthermore, the use of a common framework from the validated therapeutic trastuzumab minimizes the risk of immunogenicity in clinical applications.

The modular DATE design allows facile coupling of Fabs recognizing a variety of TAAs because most Fabs

are physically inert and can be reliably fused to a scFv without the risk of aggregation, which can arise from noncognate interactions between VH/VL domains in tandem scFv fusions.²⁵ Notably, the trastuzumab framework has proven to be highly robust for supporting many diverse paratopes, and we and others have used this framework to construct naive phage-displayed libraries that have yielded thousands of Fabs recognizing hundreds of diverse antigens.^{29,42,56–59} Consequently, virtually any stable Fab derived from natural IgGs or synthetic libraries could be converted into the DATE format to provide a vast toolkit for exploring novel TAAs for T-cell recruitment against diverse tumors.

To further enhance specificity in a modular manner, we developed d-DATES by adding a second tumor-targeting moiety in the form of an autonomous VH domain, built on a modified version of the trastuzumab framework. Autonomous VH domains are inert to interactions with Fabs and scFvs because they do not interact with VL domains and are stable and soluble on their own.^{52,60} Moreover, we show that the VH domain, which is the smallest functional antibody fragment, could be fused to the DATE without interfering with the function of either the antitumor Fab or the anti-CD3 scFv. Thus, the complementary properties of Fabs, scFvs and VH domains can be exploited to assemble DATES and d-DATES with complex biological functions, but in a facile, modular manner that ensures predictable behavior *in vitro* and *in vivo*.

To validate the DATE and d-DATE formats, we focused on developing immune T-cell redirection strategies to target pancreatic cancer, which remains recalcitrant to immunotherapy and other targeted therapies.⁶¹ Consistent with our findings at the protein level, EPHA2 was recently identified as the most highly expressed EPH family member in human PDACs by analysis of transcriptomic data from The Cancer Genome Atlas.⁶² This study also showed that EPHA2 mRNA expression was inversely correlated with patient survival and that tumor-intrinsic EPHA2 suppressed and excluded T cells from the tumor microenvironment, promoting resistance against immunotherapies. These data suggest that redirection of T cells to EPHA2 using BiTEs or DATES could potentially overcome this effect. A BiTE targeting EPHA2 was previously shown to be effective in preventing the engraftment of human colorectal cancer cells and the subsequent appearance of tumors in mice, although the cancer cells were co-injected subcutaneously with T cells.⁴⁶ Building on this and other reports suggesting that EPHA2 may be a promising target for pancreatic carcinoma,^{54,63} we showed that our potent anti-

EPHA2 DATES indeed effectively recruited T-cell cytotoxic activity to multiple PDAC lines *in vitro* and could even inhibit the growth of pre-established, rapidly growing tumors in a PDAC mouse model. These promising initial studies warrant more detailed follow-up to assess not only efficacy, but also serum half-life, biodistribution, and most importantly, toxicity and other adverse events, including cytokine release syndrome, which is the most common and severe adverse event of T-cell redirection therapies.^{64–66}

Our data demonstrated that d-DATES, targeting EPHB2 in addition to EPHA2, were at least as efficacious *in vitro* as DATES targeting only EPHA2. In combination with an anti-EPHA2 Fab, the anti-EPHB2 VH domain enhanced binding to cells that express both antigens, compared to cells that express only EPHA2. While we observed a reduction in binding for all EPHA2/B2-targeting d-DATES that we tested compared to their respective DATES to cells that express EPHA2 alone, only the A2-4/B2-1 d-DATE additionally displayed enhanced binding to WT KP4 cells compared to the A2-4 DATE, and corresponding cytotoxic efficacy. Given that A2-4 was the weakest of the EPHA2-binding Fabs, this suggests that the EPHB2-binding VH domain may enhance affinity and efficacy of the d-DATE when coupled to a lower affinity Fab. Similar function-enhancing effects driven by increased cross-arm binding efficiency have been shown for other bispecific antibodies.^{35,67} Additionally, we showed that the anti-EPHB2 VH domain in these d-DATES does not induce T-cell stimulation and consequent T-cell-mediated cytotoxicity on its own, but rather, this function is mediated via the Fab arm of the d-DATES. Therefore, these particular d-DATES do not depend on conventional “AND” logic for T-cell activation where both antigens contribute equally to the cytotoxic potential of the therapy. Instead, selectivity is conferred to dual antigen-expressing cells compared to single antigen-expressing cells

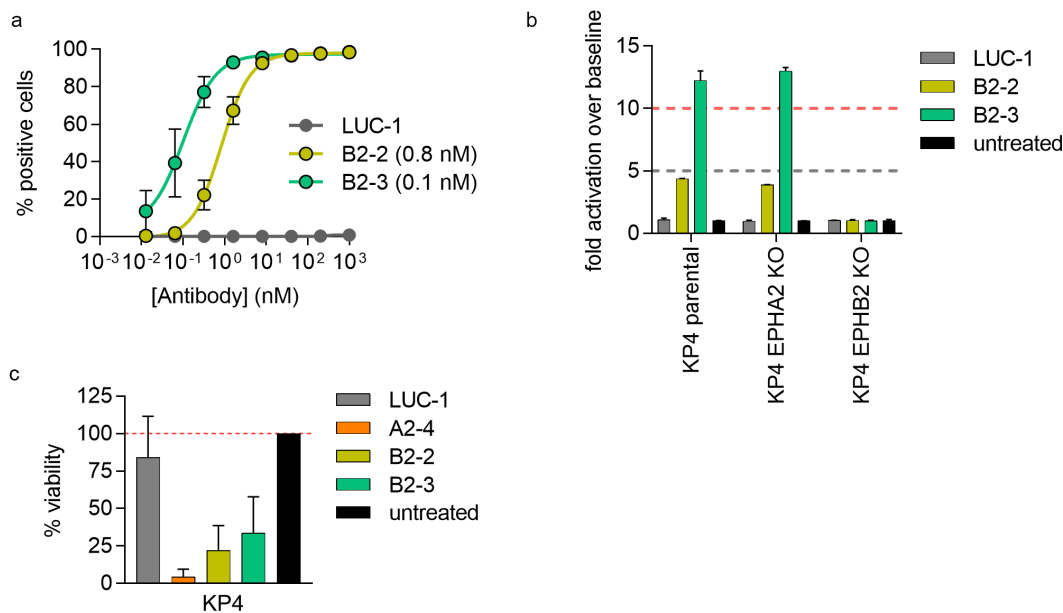


Figure 8. Characterization of EPHB2-targeting DATES. **(A)** Binding of EPHB2-targeting DATES to KP4-luciferase cells assessed by flow cytometry at various concentrations (0.013–1000 nM) (pooled from $n = 2$ independent experiments). **(B)** Jurkat TCR activation assay in response to 50 nM DATE treatment of KP4 parental, EPHA2 KO or EPHB2 KO cells (NFAT reporter assay) ($n = 2$, 2 technical replicates each). Grey and red dashed lines indicate 5- and 10-fold activation over baseline, respectively. **(C)** Viability of KP4-luciferase cells assessed by luciferase expression 3 d after treatment with 50 nM DATES in the presence of PBMCs (pooled from $n = 3$ independent experiments with PBMCs from different donors).

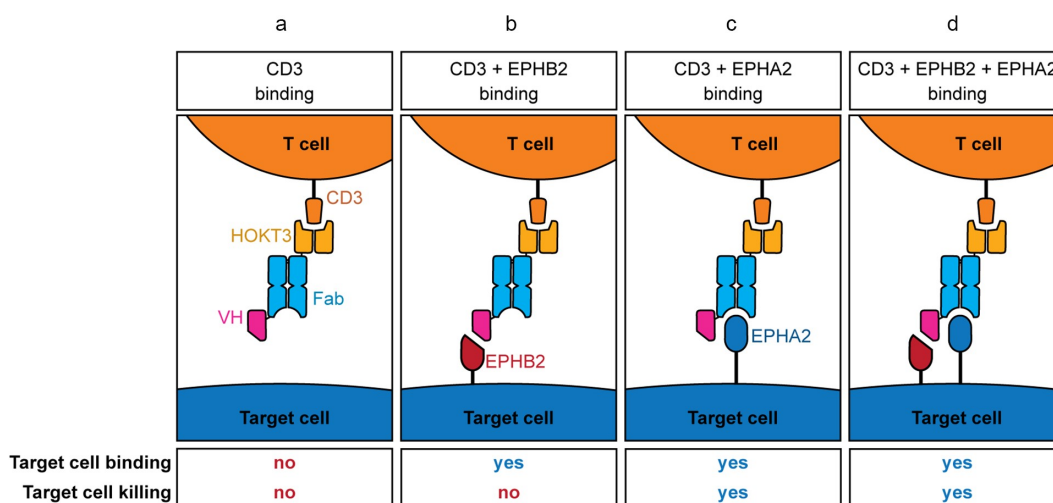


Figure 9. Schematic of cell binding and killing by d-DATES. **(A)** d-DATES that only bind to CD3 on T cells through the hOKT3 scFv arm (yellow) do not bind or kill target cells. **(B)** d-DATES that bind to target cells through the EPHB2-targeting VH domain (pink) do not kill target cells. **(C)** d-DATES that bind to EPHA2 only through the Fab (blue) cause target cell killing. **(D)** d-DATES that bind to EPHA2 and EPHB2 through the Fab and VH domain, respectively, also cause target cell killing.

through avidity effects, which can also enhance cytotoxic action that is dependent on a single antigen, as in the case of the A2-4/B2-1 d-DATE.

Thus, we report here the design of a modular antibody format that could be customized to enhance the specificity of T-cell redirection to tumors. Further evaluation of antigen pairs will allow us to evaluate the generality of these observations. Further studies will also be required to define considerations that guide effective antigen/epitope pairing to create co-accessible d-DATE targets and geometries suitable for T-cell toxicity. In particular, EPH receptors homo- and heterodimerize to create a range of conformational forms in which ectodomains either protrude perpendicular to the cell surface or potentially bend and array parallel to the cell surface.^{68,69} It is not clear which receptor conformation is preferred for engagement of DATES and d-DATES and how these conformations influence cytotoxicity.

In the case of the anti-EPHB2 B2-1 VH domain that was used as an auxiliary arm, we showed effects on binding but not killing of target cells, despite our observation that the B2-1 epitope is permissive to T-cell-mediated cytotoxicity when targeted with a DATE containing an anti-EPHB2 Fab. One explanation for the inability of the VH domain to induce killing on its own in the d-DATE format could be its lower affinity for EPHB2 compared with the Fabs in the DATE format. Alternatively, the distance between the target cell and T cell has been shown to be crucial for effective killing, with shorter distances facilitating the formation of an immunological synapse.^{16,20,21} It is likely that a target cell bound by the VH domain in a d-DATE is not in the same proximity to the T cell as a target cell bound by the Fab. However, the exact mechanism remains to be elucidated, as well as whether this property applies broadly to d-DATES. It is plausible that the function of the auxiliary arm may differ depending on the affinity and epitope of the particular VH domain and the Fab killing arm with which it is coupled. Whether other VH domains in the d-DATE format may be capable of mediating T-cell activation on their own remains to be determined. If this were the case, it

would suggest the possibility of employing “OR” logic with d-DATES to prevent antigen escape of tumor cells by promoting T-cell activation with either one of two TAAs.⁷⁰

We hypothesize that a nonkilling auxiliary arm could be used to preferentially accumulate the d-DATE in a specific tissue, where it only induces cytotoxicity when bound to the killing arm target, thereby increasing specificity and promoting a more localized T-cell response. Our data suggest that this strategy may be particularly effective with a high affinity auxiliary arm that would mainly drive targeting and a low affinity killing arm that would cause cytotoxicity and would be enhanced by cross-arm binding efficiency. Using synthetic biology, d-DATES with precisely engineered specificities and affinities may enable more targeted activation of T-cell cytotoxicity based on engagement of two distinct cell-surface markers on tumors. Thus, d-DATES can be tailored to preferentially bind cancer cells that express distinct combinations of antigens to potentially improve the efficacy and safety of T-cell redirection.

Abbreviations:

BITEs: Bispecific T cell engager
 BLI: Biolayer interferometry
 CAR: Chimeric antigen receptor
 CDR: Complementarity-determining region
 CMV: Cytomegalovirus
 DATE: Dual Antigen T-cell Engager
 d-DATE: double-DATE
 EGFRvIII: Epidermal growth factor receptor variant III
 ELISA: Enzyme-linked immunosorbent assay
 EPCAM: Epithelial cell adhesion molecule
 EPH: Ephrin receptor
 Fab: Antigen-binding fragment
 GLuc: Gaussia luciferase
 HER2: Human epidermal growth factor receptor 2
 hOKT3: humanized OKT3
 HRP: Horse radish peroxidase
 KRAS: Kirsten rat sarcoma viral oncogene homolog
 mOKT3: murine OKT3

NFAT: Nuclear factor of activated T cells
 NSG-SGM3: nonobese diabetic, severe combined immunodeficient, interleukin-2 receptor gamma null mice over-expressing human interleukin 3, granulocyte macrophage colony-stimulating factor, and stem cell factor
 PBMC: Peripheral blood mononuclear cell
 PDAC: Pancreatic ductal adenocarcinoma
 RTK: Receptor tyrosine kinase
 scFv: single-chain variable fragment
 SEC: Size-exclusion chromatography
 SDS-PAGE: sodium dodecyl sulfate-polyacrylamide gel electrophoresis
 TAA: Tumor-associated antigen
 TCR: T-cell receptor
 TIC: Tumor-initiating cell
 VH: Variable heavy-chain domain
 VL: Variable light-chain domain

Acknowledgments

The authors acknowledge the help of Lynda Ploder, Nick Jarvik and the Toronto Recombinant Antibody Centre (TRAC) for antibody selections and characterization, and Dr Jason Moffat from the Donnelly Centre, University of Toronto, for kindly providing reagents and advice. We thank Dionne White and Joanna Warzyszyńska from the University of Toronto Flow Cytometry facility for training and assistance, as well as the Pathology Research Program and the Advanced Optical Microscopy Facility of the University Health Network for immunohistochemistry and imaging. We also thank Zhenyue Hao, Leslie Dunning and the University of Toronto's Division of Comparative Medicine for assistance with animal services and experiments. This work was supported by a Terry Fox Research Institute Program Projects Grant (TFRI Project #1065) and Genome Canada grant #OGI-052.

Author contributions

LE and KHS contributed equally to this manuscript. LE, JJA, and SSS conceptualized and directed the work, and wrote the manuscript. LE performed experimental activities, data analyses, developed cell lines, and designed antibody modalities. KHS performed experimental activities, mouse studies, data analyses, and wrote and revised the manuscript. AW contributed to cell line development. MG, LLB, LC, and JJA contributed to paratope discovery and characterization. MP performed OKT3 humanization. AK provided reagents and critical insights. SSS acquired the funding and provided the resources for this work. All authors read and edited the manuscript.

Disclosure of potential conflicts of interest

No potential conflict of interest was reported by the author(s).

Funding

This work was supported by the Genome Canada [OGI-052]; Terry Fox Research Institute [1065].

ORCID

Levi L. Blazer  <http://orcid.org/0000-0001-9594-4642>

References

- Nelson MH, Paulos CM. Novel immunotherapies for hematologic malignancies. *Immunol Rev*. 2015;263(1):90–105. doi:10.1111/imr.12245.
- Weiner LM, Murray JC, Shuptrine CW. Antibody-based immunotherapy of cancer. *Cell*. 2012;148(6):1081–84. doi:10.1016/j.cell.2012.02.034.
- Strohl WR, Naso M. Bispecific T-Cell redirection versus chimeric antigen receptor (CAR)-T cells as approaches to kill cancer cells. *Antibodies (Basel)*. 2019;8(3). doi:10.3390/antib8030041.
- Slaney CY, Wang P, Darcy PK, Kershaw MH. CARs versus BiTEs: a comparison between T Cell-redirection strategies for cancer treatment. *Cancer Discov*. 2018;8(8):924–34. doi:10.1158/2159-8290.CD-18-0297.
- Cruz E, Kayser V. Monoclonal antibody therapy of solid tumors: clinical limitations and novel strategies to enhance treatment efficacy. *Biologics*. 2019;13:33–51. doi:10.2147/BTT.S166310.
- Jain RK, Baxter LT. Mechanisms of heterogeneous distribution of monoclonal antibodies and other macromolecules in tumors: significance of elevated interstitial pressure. *Cancer Res*. 1988;48:7022–32.
- Whiteside TL. The tumor microenvironment and its role in promoting tumor growth. *Oncogene*. 2008;27(45):5904–12. doi:10.1038/onc.2008.271.
- Majzner RG, Mackall CL. Tumor antigen escape from CAR T-cell therapy. *Cancer Discov*. 2018;8(10):1219–26. doi:10.1158/2159-8290.CD-18-0442.
- Sharma P, Hu-Lieskovan S, Wargo JA, Ribas A. Primary, adaptive, and acquired resistance to cancer immunotherapy. *Cell*. 2017;168(4):707–23. doi:10.1016/j.cell.2017.01.017.
- Feig C, Jones JO, Kraman M, Wells RJ, Deonaraine A, Chan DS, Connell CM, Roberts EW, Zhao Q, Ol C, others, et al. Targeting CXCL12 from FAP-expressing carcinoma-associated fibroblasts synergizes with anti-PD-L1 immunotherapy in pancreatic cancer. *Proc Natl Acad Sci U S A*. 2013;110(50):20212–17. doi:10.1073/pnas.1320318110.
- Spranger S, Bao R, Gajewski TF. Melanoma-intrinsic β -catenin signalling prevents anti-tumour immunity. *Nature*. 2015;523(7559):231–35. doi:10.1038/nature14404.
- Bonaventura P, Shekarian T, Alcazer V, Valladeau-Guilemond J, Valesia-Wittmann S, Amigorena S, Caux C, Depil S. Cold tumors: a therapeutic challenge for immunotherapy. *Front Immunol*. 2019;10:168. doi:10.3389/fimmu.2019.00168.
- Labrijn AF, Janmaat ML, Reichert JM, Parren PWHI. Bispecific antibodies: a mechanistic review of the pipeline. *Nat Rev Drug Discov*. 2019;18(8):585–608. doi:10.1038/s41573-019-0028-1.
- Kontermann RE, Brinkmann U. Bispecific antibodies. *Drug Discov Today*. 2015;20(7):838–47. doi:10.1016/j.drudis.2015.02.008.
- Wu Z, Cheung NV. T cell engaging bispecific antibody (T-BsAb): from technology to therapeutics. *Pharmacol Ther*. 2018;182:161–75. doi:10.1016/j.pharmthera.2017.08.005.
- Ellerman D. Bispecific T-cell engagers: towards understanding variables influencing the in vitro potency and tumor selectivity and their modulation to enhance their efficacy and safety. *Methods*. 2019;154:102–17. doi:10.1016/j.ymeth.2018.10.026.
- Przepiorka D, Ko CW, Deisseroth A, Yancey CL, Candau-Chacon R, Chiu HJ, Gehrke BJ, Gomez-Broughton C, Kane RC, Kirshner S, others, et al. FDA approval: blinatumomab. *Clin Cancer Res*. 2015;21(18):4035–39. doi:10.1158/1078-0432.CCR-15-0612.
- Linke R, Klein A, Seimetz D. Catumaxomab: clinical development and future directions. *MAbs*. 2010;2(2):129–36. doi:10.4161/mabs.2.2.11221.
- Runcie K, Budman DR, John V, Seetharamu N. Bi-specific and tri-specific antibodies- the next big thing in solid tumor therapeutics. *Mol Med*. 2018;24(1):50. doi:10.1186/s10020-018-0051-4.
- Li J, Stagg NJ, Johnston J, Harris MJ, Menzies SA, DiCara D, Clark V, Hristopoulos M, Cook R, Slaga D and others, et al. Membrane-Proximal epitope facilitates efficient T Cell synapse formation by Anti-FcRH5/CD3 and is a requirement for myeloma cell killing. *Cancer Cell*. 2017;31(3):383–95. doi:10.1016/j.ccell.2017.02.001.
- Bluemel C, Hausmann S, Fluhr P, Sriskandarajah M, Stallcup WB, Baeuerle PA, Kufer P. Epitope distance to the target cell membrane and antigen size determine the potency of T cell-mediated lysis by

- BiTE antibodies specific for a large melanoma surface antigen. *Cancer Immunol Immunother.* 2010;59(8):1197–209. doi:10.1007/s00262-010-0844-y.
22. Yokota T, Milenic DE, Whitlow M, Schlom J. Rapid tumor penetration of a single-chain Fv and comparison with other immunoglobulin forms. *Cancer Res.* 1992;52:3402–08.
 23. Mabry R, Snavelly M. Therapeutic bispecific antibodies: the selection of stable single-chain fragments to overcome engineering obstacles. *IDrugs.* 2010;13:543–49.
 24. Quintero-Hernández V, Juárez-González VR, Ortiz-León M, Sánchez R, Possani LD, Becerril B. The change of the scFv into the Fab format improves the stability and in vivo toxin neutralization capacity of recombinant antibodies. *Mol Immunol.* 2007;44(6):1307–15. doi:10.1016/j.molimm.2006.05.009.
 25. Wörn A, Plückthun A. Stability engineering of antibody single-chain Fv fragments. *J Mol Biol.* 2001;305(5):989–1010. doi:10.1006/jmbi.2000.4265.
 26. Leung KK, Wilson GM, Kirkemo LL, Riley NM, Coon JJ, Wells JA. Broad and thematic remodeling of the surfaceome and glycoproteome on isogenic cells transformed with driving proliferative oncogenes. *Proc Natl Acad Sci U S A.* 2020;117(14):7764–75. doi:10.1073/pnas.1917947117.
 27. Sugawa N, Ekstrand AJ, James CD, Collins VP. Identical splicing of aberrant epidermal growth factor receptor transcripts from amplified rearranged genes in human glioblastomas. *Proc Natl Acad Sci U S A.* 1990;87(21):8602–06. doi:10.1073/pnas.87.21.8602.
 28. Collins MA, Bednar F, Zhang Y, Brisset JC, Galbán S, Galbán CJ, Rakshit S, Flannagan KS, Adsay NV, Pasca Di Magliano M. Oncogenic *kras* is required for both the initiation and maintenance of pancreatic cancer in mice. *J Clin Invest.* 2012;122(2):639–53. doi:10.1172/JCI59227.
 29. Martinko AJ, Truillet C, Julien O, Diaz JE, Horlbeck MA, Whiteley G, Blonder J, Weissman JS, Bandyopadhyay S, Mj E, others, et al. Targeting RAS-driven human cancer cells with antibodies to upregulated and essential cell-surface proteins. *Elife.* 2018;7. doi:10.7554/eLife.31098.
 30. Roskopf CC, Braciak TA, Fenn NC, Kobold S, Fey GH, Hopfner KP, Oduncu FS. Dual-targeting triplebody 33-3-19 mediates selective lysis of biphenotypic CD19+ CD33+ leukemia cells. *Oncotarget.* 2016;7(16):22579–89. doi:10.18632/oncotarget.8022.
 31. Jia H, Wang Z, Wang Y, Liu Y, Dai H, Tong C, Guo Y, Guo B, Ti D, Han X and others. Haploidentical CD19/CD22 bispecific CAR-T cells induced MRD-negative remission in a patient with relapsed and refractory adult B-ALL after haploidentical hematopoietic stem cell transplantation. *J Hematol Oncol.* 2019;12(1):57. doi:10.1186/s13045-019-0741-6.
 32. Fisher J, Abramowski P, Wisidagamage Don ND, Flutter B, Capsomidis A, Cheung GW, Gustafsson K, Anderson J. Avoidance of on-target off-tumor activation using a co-stimulation-only chimeric antigen receptor. *Mol Ther.* 2017;25(5):1234–47. doi:10.1016/j.ymthe.2017.03.002.
 33. Roybal KT, Rupp LJ, Morsut L, Walker WJ, McNally KA, Park JS, Lim WA. Precision tumor recognition by T Cells with combinatorial antigen-sensing circuits. *Cell.* 2016;164(4):770–79. doi:10.1016/j.cell.2016.01.011.
 34. Banaszek A, Bumm TGP, Nowotny B, Geis M, Jacob K, Wöfl M, Trebing J, Kucka K, Kouhestani D, Gogishvili T, others, et al. On-target restoration of a split T cell-engaging antibody for precision immunotherapy. *Nat Commun.* 2019;10(1):5387. doi:10.1038/s41467-019-13196-0.
 35. Zheng S, Moores S, Jarantow S, Pardinis J, Chiu M, Zhou H, Wang W. Cross-arm binding efficiency of an EGFR x c-Met bispecific antibody. *MAbs.* 2016;8(3):551–61. doi:10.1080/19420862.2015.1136762.
 36. Slaga D, Ellerman D, Lombana TN, Vij R, Li J, Hristopoulos M, Clark R, Johnston J, Shelton A, Mai E, others, et al. Avidity-based binding to HER2 results in selective killing of HER2-overexpressing cells by anti-HER2/CD3. *Sci Transl Med.* 2018;10(463). doi:10.1126/scitranslmed.aat5775.
 37. Lu D, Jimenez X, Zhang H, Bohlen P, Witte L, Zhu Z. Fab-scFv fusion protein: an efficient approach to production of bispecific antibody fragments. *J Immunol Methods.* 2002;267(2):213–26. doi:10.1016/S0022-1759(02)00148-5.
 38. Persson H, Ye W, Wernimont A, Adams JJ, Koide A, Koide S, Lam R, Ss S. CDR-H3 diversity is not required for antigen recognition by synthetic antibodies. *J Mol Biol.* 2013;425(4):803–11. doi:10.1016/j.jmb.2012.11.037.
 39. Himanen JP, Yermekbayeva L, Janes PW, Walker JR, Xu K, Atapattu L, Rajashankar KR, Mensinga A, Lackmann M, Db N, others, et al. Architecture of Eph receptor clusters. *Proc Natl Acad Sci U S A.* 2010;107(24):10860–65. doi:10.1073/pnas.1004148107.
 40. Birtalan S, Zhang Y, Fellouse FA, Shao L, Schaefer G, Sidhu SS. The intrinsic contributions of tyrosine, serine, glycine and arginine to the affinity and specificity of antibodies. *J Mol Biol.* 2008;377(5):1518–28. doi:10.1016/j.jmb.2008.01.093.
 41. Lobo NC, Gedye C, Apostoli AJ, Brown KR, Paterson J, Stickle N, Robinette M, Fleshner N, Hamilton RJ, Kulkarni G, others, et al. Efficient generation of patient-matched malignant and normal primary cell cultures from clear cell renal cell carcinoma patients: clinically relevant models for research and personalized medicine. *BMC Cancer.* 2016;16(1):485. doi:10.1186/s12885-016-2539-z.
 42. Nixon AML, Duque A, Yelle N, McLaughlin M, Davoudi S, Pedley NM, Haynes J, Brown KR, Pan J, Hart T, others, et al. A rapid in vitro methodology for simultaneous target discovery and antibody generation against functional cell subpopulations. *Sci Rep.* 2019;9(1):842. doi:10.1038/s41598-018-37462-1.
 43. Steinhart Z, Pavlovic Z, Chandrashekar M, Hart T, Wang X, Zhang X, Robitaille M, Brown KR, Jaksani S, Overmeer R, others, et al. Genome-wide CRISPR screens reveal a Wnt-FZD5 signaling circuit as a druggable vulnerability of RNF43-mutant pancreatic tumors. *Nat Med.* 2017;23(1):60–68. doi:10.1038/nm.4219.
 44. Ran FA, Hsu PD, Wright J, Agarwala V, Scott DA, Zhang F. Genome engineering using the CRISPR-Cas9 system. *Nat Protoc.* 2013;8(11):2281–308. doi:10.1038/nprot.2013.143.
 45. Fu X, Tao L, Rivera A, Williamson S, Song XT, Ahmed N, Zhang X. A simple and sensitive method for measuring tumor-specific T cell cytotoxicity. *PLoS One.* 2010;5(7):e11867. doi:10.1371/journal.pone.0011867.
 46. Hammond SA, Lutterbuese R, Roff S, Lutterbuese P, Schlereth B, Bruckheimer E, Kinch MS, Coats S, Baeuerle PA, Kufer P, others, et al. Selective targeting and potent control of tumor growth using an EphA2/CD3-bispecific single-chain antibody construct. *Cancer Res.* 2007;67(8):3927–35. doi:10.1158/0008-5472.CAN-06-2760.
 47. Li N, Liu S, Sun M, Chen W, Xu X, Zeng Z, Tang Y, Dong Y, Chang AH, Zhao Q. Chimeric antigen receptor-modified T Cells redirected to EphA2 for the immunotherapy of non-small cell lung cancer. *Transl Oncol.* 2018;11(1):11–17. doi:10.1016/j.tranon.2017.10.009.
 48. Iwahori K, Kakarla S, Velasquez MP, Yu F, Yi Z, Gerken C, Song XT, Gottschalk S. Engager T cells: a new class of antigen-specific T cells that redirect bystander T cells. *Mol Ther.* 2015;23(1):171–78. doi:10.1038/mt.2014.156.
 49. Brischwein K, Schlereth B, Guller B, Steiger C, Wolf A, Lutterbuese R, Offner S, Locher M, Urbig T, Raum T, others, et al. MT110: a novel bispecific single-chain antibody construct with high efficacy in eradicating established tumors. *Mol Immunol.* 2006;43(8):1129–43. doi:10.1016/j.molimm.2005.07.034.
 50. Herrmann I, Baeuerle PA, Friedrich M, Murr A, Filusch S, Rüttinger D, Majdoub MW, Sharma S, Kufer P, Raum T, others, et al. Highly efficient elimination of colorectal tumor-initiating cells by an EpCAM/CD3-bispecific antibody engaging human T cells. *PLoS One.* 2010;5(10):e13474. doi:10.1371/journal.pone.0013474.
 51. Huang J, Li C, Wang Y, Lv H, Guo Y, Dai H, Wicha MS, Chang AE, Li Q. Cytokine-induced killer (CIK) cells bound with anti-CD3/anti-CD133 bispecific antibodies target CD133(high) cancer stem cells in vitro and in vivo. *Clin Immunol.* 2013;149(1):156–68. doi:10.1016/j.clim.2013.07.006.

52. Ma X, Barthelemy PA, Rouge L, Wiesmann C, Sidhu SS. Design of synthetic autonomous VH domain libraries and structural analysis of a VH domain bound to vascular endothelial growth factor. *J Mol Biol.* 2013;425(12):2247–59. doi:10.1016/j.jmb.2013.03.020.
53. Mudali SV, Fu B, Lakkur SS, Luo M, Embuscado EE, Iacobuzio-Donahue CA. Patterns of EphA2 protein expression in primary and metastatic pancreatic carcinoma and correlation with genetic status. *Clin Exp Metastasis.* 2006;23(7–8):357–65. doi:10.1007/s10585-006-9045-7.
54. Duxbury MS, Ito H, Zinner MJ, Ashley SW, Whang EE. EphA2: a determinant of malignant cellular behavior and a potential therapeutic target in pancreatic adenocarcinoma. *Oncogene.* 2004;23(7):1448–56. doi:10.1038/sj.onc.1207247.
55. Pw J, Griesshaber B, Atapattu L, Nievergall E, Li H, Mensinga A, Chheang C, Bw D, Aw B, Pi B, others, et al. Eph receptor function is modulated by heterooligomerization of A and B type Eph receptors. *J Cell Biol.* 2011;195(6):1033–45. doi:10.1083/jcb.201104037.
56. Fellouse FA, Esaki K, Birtalan S, Raptis D, Cancasci VJ, Koide A, Jhurani P, Vasser M, Wiesmann C, Aa K, others, et al. High-throughput generation of synthetic antibodies from highly functional minimalist phage-displayed libraries. *J Mol Biol.* 2007;373(4):924–40. doi:10.1016/j.jmb.2007.08.005.
57. Miersch S, Kuruganti S, Walter MR, Sidhu SS. A panel of synthetic antibodies that selectively recognize and antagonize members of the interferon alpha family. *Protein Eng Des Sel.* 2017;30(9):697–704. doi:10.1093/protein/gzx048.
58. Pollock SB, Hu A, Mou Y, Martinko AJ, Julien O, Hornsby M, Ploder L, Adams JJ, Geng H, Müschen M, others, et al. Highly multiplexed and quantitative cell-surface protein profiling using genetically barcoded antibodies. *Proc Natl Acad Sci U S A.* 2018;115(11):2836–41. doi:10.1073/pnas.1721899115.
59. Tao Y, Mis M, Blazer L, Ustav M, Steinhart Z, Chidiac R, Kubarakos E, O'Brien S, Wang X, Jarvik N, others, et al. Tailored tetravalent antibodies potently and specifically activate Wnt/frizzled pathways in cells, organoids and mice. *Elife.* 2019;8. doi:10.7554/eLife.46134.
60. Ward ES, Güssow D, Griffiths AD, Jones PT, Winter G. Binding activities of a repertoire of single immunoglobulin variable domains secreted from escherichia coli. *Nature.* 1989;341(6242):544–46. doi:10.1038/341544a0.
61. Hilmi M, Bartholin L, Neuzillet C. Immune therapies in pancreatic ductal adenocarcinoma: where are we now?. *World J Gastroenterol.* 2018;24(20):2137–51. doi:10.3748/wjg.v24.i20.2137.
62. Markosyan N, Li J, Sun YH, Richman LP, Lin JH, Yan F, Quinones L, Sela Y, Yamazoe T, Gordon N, others, et al. Tumor cell-intrinsic EPHA2 suppresses anti-tumor immunity by regulating PTGS2 (COX-2). *J Clin Invest.* 2019;129(9):3594–609. doi:10.1172/JCI127755.
63. Wu B, Wang S, De SK, Barile E, Quinn BA, Zharkikh I, Purves A, Stebbins JL, Oshima RG, Pb F, others, et al. Design and characterization of novel EphA2 agonists for targeted delivery of chemotherapy to cancer cells. *Chem Biol.* 2015;22(7):876–87. doi:10.1016/j.chembiol.2015.06.011.
64. Topp MS, Gökbuget N, Zugmaier G, Klappers P, Stelljes M, Neumann S, Viardot A, Marks R, Diedrich H, Faul C, others, et al. Phase II trial of the anti-CD19 bispecific T cell-engager blinatumomab shows hematologic and molecular remissions in patients with relapsed or refractory B-precursor acute lymphoblastic leukemia. *J Clin Oncol.* 2014;32(36):4134–40. doi:10.1200/JCO.2014.56.3247.
65. Maude SL, Frey N, Shaw PA, Aplenc R, Barrett DM, Bunin NJ, Chew A, Gonzalez VE, Zheng Z, Sf L, others, et al. Chimeric antigen receptor T cells for sustained remissions in leukemia. *N Engl J Med.* 2014;371(16):1507–17. doi:10.1056/NEJMoa1407222.
66. Davila ML, Riviere I, Wang X, Bartido S, Park J, Curran K, Chung SS, Stefanski J, Borquez-Ojeda O, Olszewska M, others, et al. Efficacy and toxicity management of 19-28z CAR T cell therapy in B cell acute lymphoblastic leukemia. *Sci Transl Med.* 2014;6(224):224ra25. doi:10.1126/scitranslmed.3008226.
67. Harms BD, Kearns JD, Iadevaia S, Lugovskoy AA. Understanding the role of cross-arm binding efficiency in the activity of monoclonal and multispecific therapeutic antibodies. *Methods.* 2014;65:95–104.
68. Himanen JP. Ectodomain structures of Eph receptors. *Semin Cell Dev Biol.* 2012;23(1):35–42. doi:10.1016/j.semcdb.2011.10.025.
69. Chavent M, Seiradake E, Jones EY, Sansom MS. Structures of the EphA2 receptor at the membrane: role of lipid interactions. *Structure.* 2016;24(2):337–47. doi:10.1016/j.str.2015.11.008.
70. Zah E, Nam E, Bhuvan V, Tran U, Ji BY, Gosliner SB, Wang X, Brown CE, Chen YY. Systematically optimized BCMA/CS1 bispecific CAR-T cells robustly control heterogeneous multiple myeloma. *Nat Commun.* 2020;11(1):2283. doi:10.1038/s41467-020-16160-5.